University of Alberta

Development of Engineered Micro-Particles via Spray Drying
for Respiratory Drug Delivery

by

Sadaf Matinkhoo

A thesis submitted to the Faculty of Graduate Studies and Research
in partial fulfillment of the requirements for the degree of

Master of Science

Department of Mechanical Engineering

Fall 2013
Edmonton, Alberta

Abstract

In this study, respirable dry powders for the treatment of *Pseudomonas aeruginosa* and *Burkholderia cepacia* complex infections in cystic fibrosis patients were developed. The feasibility of spray drying aqueous solutions containing bacteriophages was investigated. Bacteriophages KS4-M, KS14 and ΦKZ/D3 cocktail (active against *P. aeruginosa* or *Burkholderia cepacia*) were spray dried in solutions containing other excipients including trehalose and L-leucine. Acceptable process loss (0.4-0.8 log pfu), high delivery efficiency (69.7% of capsule load for the lead formulation), and desirable particle size (2.5-2.8 μm MMAD) were achieved. Then, L-leucine was substituted by and tested against D-leucine in the lead formulation to help eradicate bacteria biofilms. Similar morphologies and MMADs (3.25±0.03 μm and 3.82±0.04 μm for D- and L-leucine/trehalose) were achieved. Both formulations had acceptable total lung mass fractions (62.0±7.81% and 63.66±16.37% of emitted mass for D- and L-leucine/trehalose). Substitution L-leucine with D-leucine was found to be feasible.

Acknowledgements

"Little by little, one travels far."
J.R.R. Tolkien

Now that my journey is over, I look back at the path, and I know I could not have come so far if not for all the help and support I had. I have so many people to thank:

Dr. Reinhard Vehring, whose extensive knowledge and enthusiasm made this research and thesis possible. His patience and encouragements helped me believe in myself, and I will always be grateful for that.

My thesis committee members, Dr. Warren Finlay and Dr. Aloke Kumar, for their insightful comments.

Dr. Jonathan Dennis, Karlene Lynch, and Mandie Goudie in the Department of Biological Sciences, and Helena Orszanska in the Department of Mechanical Engineering for their sincere cooperation in this research.

My friends and labmates in Particle Engineering laboratory in the Mechanical Engineering Department, specially Susan Hoe, Mohammed Boraey, James Ivey, and Abouzar Shamsaddini. This thesis would not have been possible without their kind help.

My dearest mom and dad, and my sweet brother. They kept me going even when I felt I couldn't take one more step. I can never thank them enough.

And finally, my beloved Hootan, who stood by my side in every step and never gave up on me. I feel truly blessed to know and love him.

Thank you all.

Contents

List of Tables

List of Figures

Nomenclature

$c_{0,i}$	Initial concentration of component i
$c_{m,i}$	Average concentration of component i
$c_{s,i}$	Surface concentration of component i
$c_{sol,i}$	Solubility of component i
C_{ag}	Specific heat of atomization gas
C_c	Cunningham slip correction factor
C_{dg}	Specific heat of drying gas
C_F	Feed concentration
C_s	Specific heat of feed solution
d_0	Initial diameter
d_a	Aerodynamic diameter
d_D	Droplet diameter
d_V	Volume equivalent diameter
D_i	Diffusion coefficient of component i
E_i	Surface enrichment of component i
H_{ag}	Enthalpy of atomizing gas
H_{dg}	Enthalpy of drying gas
H_L	Heat loss
H_{sol}	Enthalpy of feed solution
K	Interaction coefficient
m_{ag}	Mass flow rate of atomizing gas
m_{dg}	Mass flow rate of drying gas
m_p	Particle mass
m_{sol}	Mass flow rate of feed solution
M_{ag}	Molecular weight of the atomizing gas
M_{dg}	Molecular weight of the drying gas

M_{sol}	Molecular weight of the feed solution
$P_{chamber}$	Absolute pressure in the drying chamber
$P^*_{T,out}$	Solvent saturation pressure at the temperature T_{out}
Pe_i	Peclet number of component i
RH	Relative humidity
$S_{0.i}$	Initial supersaturation of component i
t	Time
T_{feed}	Temperature of the feed solution
T_G	Glass transition temperature
T_{in}	Temperature of the entering drying gas
T_{out}	Temperature of the exhaust drying gas
V_D	Droplet volume
V_p	Particle volume
x_s	Solid mass fraction in the feed solution
Y_i	Mass fraction of component i
κ	Evaporation rate
ρ_b	Bulk density
ρ_p	Particle density
ρ_T	True density
ρ^*	Reference density
τ_D	Characteristic drying time
$\tau_{sat,i}$	Characteristic time to saturation for component i
χ	Dynamic shape factor
ΔH_{vap}	Solvent's latent heat of evaporation

1. Introduction

Dry powders have been used as pharmaceuticals in several forms: they have been pressed into tablets or filled into capsules for oral administration, inhaled as aerosols, or administered intranasally [1]. Administration of dry powders via inhalation is a common way of targeted drug delivery, i.e., delivering the drug to the site of action. In contrast to the conventional drug delivery methods, in which the drug is usually delivered to the diseased tissue or organ via blood circulation, targeted drug delivery methods aim only for the tissues of interest. This helps to deliver higher concentrations of the drug to where it actually is needed rather than distributing the drug throughout the body and having limited control on what portion of it will reach the diseased tissue. Delivering higher concentrations of the drug to the site of action in each administration reduces the frequency that the drug needs to be administered and also reduces the fluctuation of the concentration of the drug existing in the blood. Moreover, delivering the drug to only specific parts of the body can dramatically reduce its side effects [2].

Inhalation, amongst other drug administration routes, has a number of advantages: it results in rapid delivery of high concentrations of the drug over a large surface area in the respiratory tract; it allows small molecules to pass since the lung membrane is very permeable; and it exposes the drug to much less metabolism and degradation compared with other routes of administration [3–5]. Moreover, it is a noninvasive administration method which needs no professional supervision in most cases. The downside of drug administration via inhalation is the need for specifically-designed particles.

Microparticles are the building blocks of therapeutic aerosols for inhalation [6]. The approach towards the function of micro-particles has recently

changed with the growing need to develop more advanced therapeutics: they are no longer viewed as merely carriers of drugs but rather as sophisticated dosage forms with multiple functions such as delivering and stabilizing the therapeutic agents through being designed to have desirable size, texture, and internal structure. The ability to control particle formation to achieve the required functions calls for a deep understanding of the process itself combined with the knowledge of other sciences such as chemistry and microbiology [1].

Micro-particles can be developed through several methods which are divided into two broad categories: bottom-up, in which the particles are built from smaller units, and top-down, in which the particles are manufactured through breaking down the larger units. Bulk drying processes e.g. vacuum drying and freeze drying belong to the bottom-up category. These methods usually need some kind of post-drying process such as micronization done on their final product to reach the desirable size. Spray drying, on the contrary, results in products with desirable properties in only one step.

There are several requirements for particles developed for pulmonary delivery via spray drying. First, they should be of the desirable size: 5-10μm for delivery via airways and 1-5μm for deep lung delivery [3]. Second, the particles should have low surface energy and cohesion forces to be able to aerosolize efficiently. And finally, they should be composed of material compatible with the lung tissue [7].

1.1. Spray Drying Process

Spray drying is the process of transforming a feed in the form of solution or suspension into dry powder form by exposing a spray of the feed to a drying medium. This process can be divided into several consecutive stages: atomization of the feed, exposing the atomized feed to hot drying gas,

moisture evaporation which results in dry powder, and powder recovery. Details on the theory of spray drying can be found in several sources [8, 9]. The following sections provide a summary of the theory.

1.1.1. Atomization

Atomization is the process of breaking up the liquid into droplets and forming a spray. The energy required to break up the liquid is supplied in one of centrifugal, kinetic, pressure, or sonic forms depending on the type of atomizer. The selection of the atomizer most suitable for the purpose of spray drying is of great importance in terms of the atomization efficiency. The atomizer should produce a spray with proper feed rate and droplet size to achieve the desirable properties in the final product.

Rotary atomizers exist in two forms: wheels and discs. They mostly use centrifugal energy to break up the liquid feed and can atomize high feed rates. Nozzle atomizers use pressure, kinetic, or sonic energy. They can only handle low feed rates; hence, more than one is used when higher feed rates are required.

Figure 1 shows a schematic of the liquid spray from a rotary atomizer. In this type of atomizers, the liquid enters the center of a disc or a wheel rotating at high speed and accelerates towards and out of the periphery disintegrating and forming a spray. The characteristics of the spray depend on the atomizer design and speed as well as the feed rate and properties of the feed liquid.

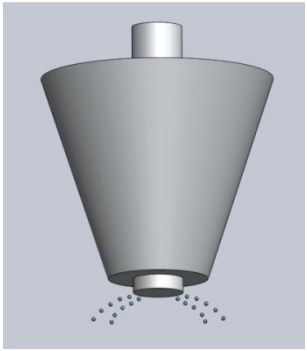

Figure 1 - Spray from a rotary atomizer, inspired by [10]

Figure 2 illustrates a schematic of the spray from a pressure nozzle. In this type of atomizers, the liquid is fed into the center of the nozzle at a high pressure. The pressure is then converted into kinetic energy, resulting in the liquid leaving the nozzle at a high speed and disintegrating instantly. The spray will form a cone outside the nozzle since the feed circulates in the atomizer. The spray from this type of atomizers is usually coarser than that of the rotary atomizers and can change depending on the atomization pressure.

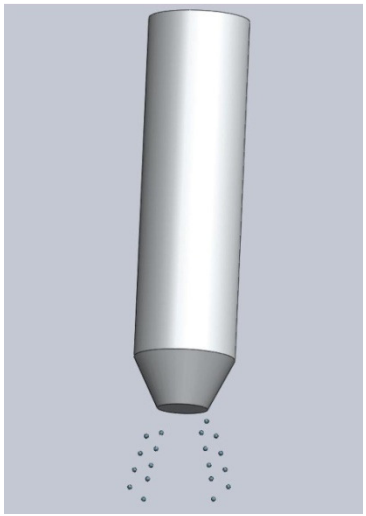

Figure 2 - Spray from a pressure nozzle atomizer, inspired by [11]

Two-fluid nozzles are another category of atomizers in which the liquid and the atomizing gas enter the nozzle separately. The kinetic energy of the high-speed atomizing gas disintegrates the liquid either inside the nozzle or when the liquid leaves the orifice – internal and external mixing. Figure 3 illustrates the structure of a two-fluid nozzle with internal (left) and external (right) mixing. A number of parameters such as the liquid feed rate and the atomization gas flow rate affect the properties of the resulting spray.

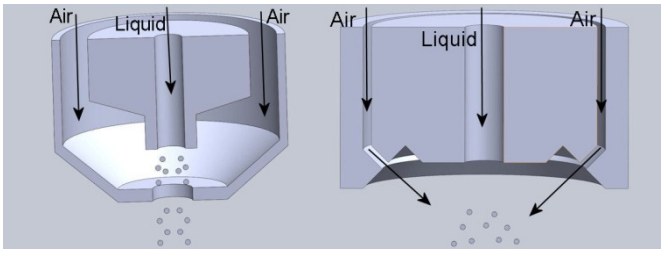

Figure 3 - Two-fluid nozzle, inspired by [12]

There are also other types of atomizers which use other forms of energy to break up the feed liquid. For instance, sonic and vibrating atomizers are usually used to atomize liquids in early stages of product development. The spray dryer used in this study (Büchi B-90) utilizes a vibrating mesh that fits into this category of atomizers.

While the droplet sizes achieved by rotary and pressure atomizers are too large for respiratory applications, two-fluid nozzles and sonic and vibrating atomizers have been frequently used in pharmaceutical industry.

1.1.2. Spray-Air Contact

Spray-air contact, which has a strong influence on the characteristics of the final product, is the next stage in spray drying process and depends on the position of the atomizer in the drying medium. Figure 4 shows two different modes of spray drying in terms of position of the atomizer in relation to the drying gas. The co-current flow configuration (left hand side) represents the mode where the atomized spray and the drying gas enter the drying medium in the same direction, while they pass the drying medium in the opposite direction in the countercurrent flow.

Co-current flow mode is most suitable for heat-sensitive material, such as bacteriophages used in this study, when short-time heat exposure is desirable and low temperature is maintained in spite of the very hot drying gas.

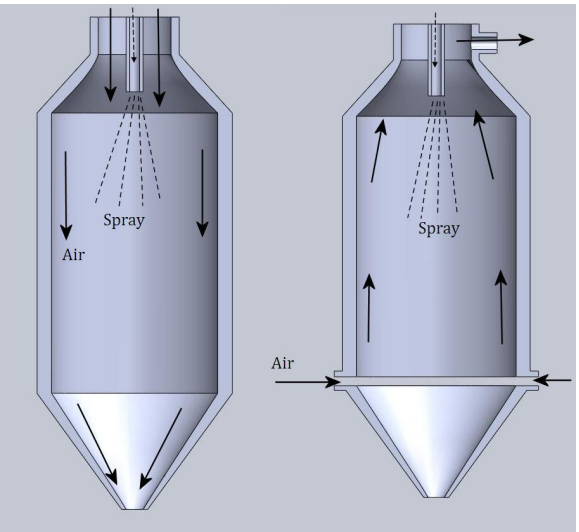

Figure 4 – Co-current and counter-current spray-air contact, inspired by [13]

The countercurrent flow (right hand side) results in a better use of the heat provided by the drying gas but expose the driest particles to the hottest gas. Nozzle atomizers are best suitable for this configuration since the upward gas flow increases the evaporation time for large droplets. Mixed flow is a combination of both co-current and countercurrent flows.

1.1.3. Solvent Evaporation

Solvent evaporation is the next stage of spray drying where particles with desirable moisture are achieved due to the contact between the spray and the hot drying gas. The rate of moisture evaporation from the droplet depends on the temperature and humidity of the drying gas as well as the droplet size, velocity, and physical properties.

1.1.4. Powder Recovery

The final product of the spray drying process is collected using cyclones, bag filters, electrostatic precipitators, or other means of powder recovery. This process can be done in either one or two stages. The choice of equipment depends on the cost, efficiency, and powder properties. While cyclones and

electrostatic precipitators are usually less efficient than bag filters, very high maintenance costs of bag filters makes them less desirable unless the dry product is so expensive that the maintenance cost is less than the cost of the potential powder loss in recovery stage. Electrostatic precipitators have high price but very low operation cost with acceptable efficiency (up to 99%) for fine particles recovery. They can operate under high temperatures and low humidity exhaust air.

There are two main spray drying configurations: open cycle and closed cycle. The difference between these two configurations is that the drying gas is exhausted after filtration in open cycle while it is re-pressurized and re-used in closed cycle. A clean filtered exhaust is needed in open-cycle to prevent the discharge of airborne powder into the surrounding air.

Spray drying was first mentioned in 1865 [8], and has had numerous applications since then. Many household products e.g. pharmaceuticals and cosmetics have either been spray dried or had a spray drying stage in their production process. Spray dryers were first used in industry to produce dry milk and detergent and were especially well-established as a one-step economic method during the Second World War when massive amount of dry food was needed.

It has been shown [1] that excipients' properties and process parameters in spray drying determine the morphology of the final product. The need for an engineering method to develop the particles has emerged since there are too many parameters involved in the process to employ an empirical approach. Moreover, using engineering methods helps design particles with desired properties for specific purposes e.g. high dispersibility for respirable dry powders.

1.2. Particle Engineering Theory and Terminology

One of the important parameters in respiratory applications of a dry powder is the particle size. The reason for this is that all the mechanisms contributing to particle deposition in respiratory tract are mainly affected by particle size and inhalation flow rate along with other parameters such as breathing pattern [7]. Only particles in a specific size range can actually make it all the way to the lungs. This size range is between 1 μm and 5 μm for dry powder particles [3]. Particles smaller than 1μm can be exhaled after inhalation and particles larger than 5μm deposit on the respiratory tract wall somewhere on their way to the lungs [3].

Particles with aspect ratios close to one are considered spherical despite having irregular shapes. This is the case with most spray dried particles i.e. they might be wrinkled or have other irregular shapes but their aspect ratios are mostly close to one [14]. Hence, their size can be specified using only their diameter; although, one should define an equivalent diameter since the particles are not perfect spheres. Several types of equivalent diameters have been introduced depending on the application. The one used more often in respiratory applications is aerodynamic diameter which is defined as the diameter of a sphere with density of 1 g/cm^3 which has the same settling velocity (the velocity that a particle reaches when settling in a fluid) as the investigated particle [15]. Equation 1 describes this diameter.

$$\boldsymbol{d_a} = \sqrt{\frac{\boldsymbol{\rho_p}}{\boldsymbol{\rho^*}}}\,\boldsymbol{d_V} \qquad (1)$$

In this equation, d_a and ρ^* are the particle aerodynamic diameter and the reference density (1 g/cm^3) respectively. To define other parameters of this equation, accurate definition of the particle volume is required. The volume of a non-spherical particle can be calculated in three different approaches regarding its voids: volume of the particle including (1) all external and

internal voids i.e. hydrodynamic volume, (2) only internal voids, and (3) neither external nor internal voids [16, 17].

For non-continuum regime, which may apply to submicron particles, Cunningham slip correction factor (C_c) must be included in equation 1. The dynamic shape factor (χ) in equation 2, which is the ratio of the actual drag force on the particle to the drag force on a sphere with the same hydrodynamic volume, is assumed to be one. For submicron particles, the Cunningham slip correction factor varies rapidly by diameter, but for particles larger than 1μm, the ratio of the two C_c's in equation 2 can be assumed to be one [17], and equation 2 can be summarized to equation 1.

$$\boldsymbol{d_a = \sqrt{\frac{\rho_p C_C(d_V)}{\rho^* C_c(d_a)} \cdot \frac{1}{\chi}}\, d_V} \qquad (2)$$

The volume equivalent diameter, d_V, which is the diameter of a perfect sphere with the same volume as the particle, can be calculated based on the hydrodynamic volume of the particle (V_p) using the equation below:

$$\boldsymbol{\frac{\pi}{6} {d_V}^3 = V_p \quad \Rightarrow \quad d_V = \sqrt[3]{\frac{6V_P}{\pi}}} \qquad (3)$$

The same definitions for volume mentioned above are used to calculate three different densities of a non-spherical particle: particle density (ρ_p), bulk density (ρ_b), and true density (ρ_T) based on first, second, and third definitions of volume respectively.

The aerodynamic diameter calculated based on the volume equivalent diameter is of great importance since it determines the particle's behavior in

an airborne aerosol. Particles with the same aerodynamic diameter have the same behavior and vice versa. Knowing the aerodynamic diameter is one of the parameters that allow us to determine whether or not the particle will deposit in the respiratory tract.

According to the mass conservation calculations below, the volume equivalent diameter can be described as a function of the droplet diameter, d_D:

$$\boldsymbol{V_D = \frac{\pi}{6} d_D{}^3} \quad (4)$$

$$\boldsymbol{m_p = \frac{\pi}{6} d_D{}^3 C_F} \quad (5)$$

$$\boldsymbol{\frac{\pi}{6} d_V{}^3 \rho_p = \frac{\pi}{6} d_D{}^3 C_F} \quad (6)$$

$$\boldsymbol{d_V = \sqrt[3]{\frac{C_F}{\rho_p}}\, d_D} \quad (7)$$

Where m_P, and C_F are particle mass and feed concentration respectively. Hence, the aerodynamic diameter can be described as a function of the feed concentration and the droplet diameter:

$$\boldsymbol{d_a = \sqrt[6]{\frac{\rho_p}{\rho^*}} \sqrt[3]{\frac{C_F}{\rho^*}}\, d_D} \quad (8)$$

This equation also demonstrates that in cases where the particle density is close to 1 g/cm^3, the particle aerodynamic diameter is only a weak function of the particle density. It also draws attention to limitations on the feed concentration to the atomizer since particle aerodynamic diameter increases with feed concentration, which is unfavorable in pulmonary applications.

Equation 9, which is another configuration of equation 8, can be used to determine the required feed concentration for spray drying any formulation

according to the target particle aerodynamic diameter and particle density, and the droplet diameter, which is determined by the atomizer properties.

$$C_F = \rho^* \sqrt{\frac{\rho^*}{\rho_p}} \left(\frac{d_a}{d_D}\right)^3 \quad (9)$$

With d_0 as the initial droplet diameter, the droplet diameter can be described as a function of time and evaporation rate [18]:

$$d^2(t) = {d_0}^2 - \kappa t \quad (10)$$

Assuming that the drying gas and the droplet temperature remain constant during most of the evaporation process and neglecting the rapid temperature change at the beginning of the process, the evaporation rate can be considered constant to simplify further calculations. This model does not capture the changes in evaporation rate right before particle solidification begins.

The drying time of the droplet, which can also be perceived as the droplet lifetime, can be derived directly from the above equation [1]:

$$\tau_D = \frac{{d_0}^2}{\kappa} \quad (11)$$

This is a very important characteristic time in the drying process since it determines how much time the droplet can spend in the drying chamber before chemical degradation happens.

Assuming a spherical shape for spray dried particles, one must be able to control the radial distribution of different components in the droplet throughout the drying process. There are a number of phenomena that could contribute to determining this distribution. Surface activity might cause a

diffusional flux towards the surface as opposed to the particle's receding surface as the solvent evaporates, which results in a higher concentration on the surface, and thus, a diffusional flux away from the surface. The combined effects of these phenomena determine the radial distribution of the components in the droplet. A dimensionless number, the Peclet number, incorporating the evaporation rate and diffusion coefficient, can be used to predict the components' distribution in a drying droplet [19]:

$$\boldsymbol{Pe_{\mathrm{i}}} = \frac{\boldsymbol{\kappa}}{\boldsymbol{8D_{\mathrm{i}}}} \qquad (12)$$

In the above equation, Pe_{i} is the *Pe* number and D_{i} the diffusion coefficient of the component i, and κ is the evaporation rate of the droplet. *Pe* number can highly affect the particle formation mechanism. For *Pe* numbers smaller than 1, the diffusional motion of the solutes existing in the droplet is fast compared to the receding speed of the droplet surface. Hence, they can move relatively quickly and distribute evenly throughout the droplet evaporation process and keep the surface enrichment –the ratio of surface concentration to average concentration of the solutes in the droplet as shown in equation 12- low. In this equation, E_{i}, $c_{\mathrm{s,i}}$, and $c_{\mathrm{m,i}}$ are surface enrichment, surface concentration, and average concentration of component i respectively [1].

$$\boldsymbol{E_{\mathrm{i}}} = \frac{\boldsymbol{c_{\mathrm{s,i}}}}{\boldsymbol{c_{\mathrm{m,i}}}} \qquad (13)$$

In case the solutes are highly soluble in the solvent, the initial supersaturation is also low, resulting for the droplet's characteristic time for the solutes to reach saturation be close to the droplet's drying time. Solid particles with a density close to the true density of the components are the result of this type of particle formation. Equations 14 and 15 are used to calculate initial supersaturation ($S_{0,\mathrm{i}}$) and time to saturation ($\tau_{\mathrm{sat,i}}$) of

component i based on initial concentration ($c_{0,i}$) and solubility ($c_{sol,i}$) of component i [1].

$$S_{0,i} = \frac{c_{0,i}}{c_{sol,i}} \quad (14)$$

$$\tau_{sat,i} = \tau_D\left(1 - (S_{0.i} \cdot E_i)^{\frac{2}{3}}\right) \quad (15)$$

For high Peclet numbers, the droplet surface recedes faster than the diffusional motion of the solutes, resulting in the solute with high Pe number accumulating on the surface and forming a shell depending on the properties of the solute molecules. Several morphologies including hollow spheres can be achieved through this type of particle formation. Figure 5 demonstrates a schematic of particle formation for high Peclet numbers.

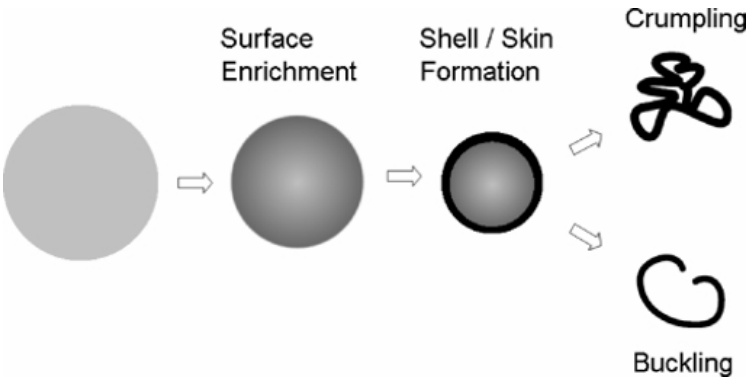

Figure 5 - Particle formation for high Peclet numbers. Figure 3 from [1], with kind permission from Springer Science and Business Media.

In reality, the Peclet number changes through the droplet evaporation process since the diffusion coefficient and the evaporation rate are not constant and vary with the droplet composition. It also changes when phase transition happens e.g. in crystallization cases. In this type of particle formation, a component with initially low Peclet number distributes evenly throughout the droplet until reaching supersaturation and then introduces a separate phase. At this point, the mobility of the component molecules is

determined by mobility of the separated phase rather than the diffusional coefficient, which results in a high Peclet number. This component then accumulates on the surface and forms a shell which may later deform into different shapes.

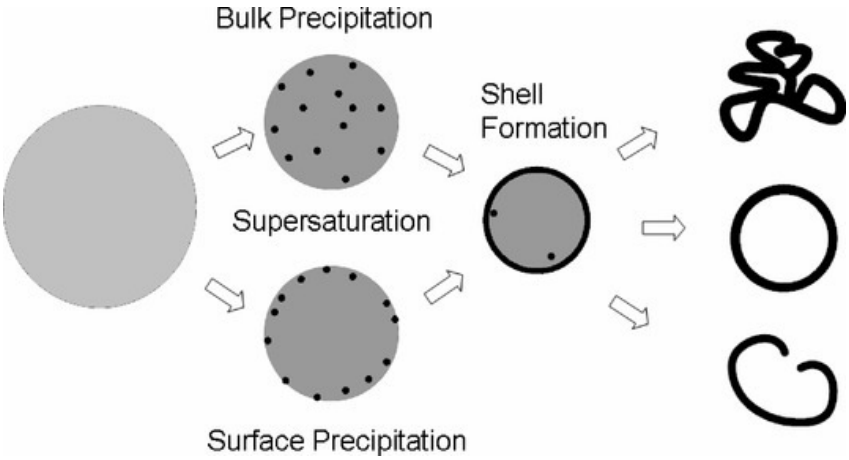

Figure 6 - Particle formation for changing Peclet numbers. Figure 5 from [1], with kind permission from Springer Science and Business Media.

The glass transition temperature (the temperature at which an amorphous solid undergoes significant changes in its material properties) of the excipients is also a very important parameter which affects the state of the final product in terms of crystallinity, and chemical and physical stability of the dry powder. Amorphous glasses tend to be physically stable when kept well below their glass transition temperature. Glass stabilizations is also used to chemically stabilize active pharmaceutical ingredients [1]. Glass transition temperature (T_G) of a mixture of two components with mass fractions of Y_1 and Y_2, interaction coefficient of K, and glass transition temperatures of $T_{G,1}$ and $T_{G,2}$ can be calculated using the Gordon-Taylor equation [20]:

$$\boldsymbol{T_{G,mixture}} = \frac{\boldsymbol{Y_1 T_{G,1} + K Y_2 T_{G,1}}}{\boldsymbol{Y_1 + K Y_2}} \quad (16)$$

Assuming K=$T_{G,1}/T_{G,2}$, this equation can be summarized in the form of Fox equation [20]:

$$\boldsymbol{T_{G,mixture}} \approx \frac{\mathbf{1}}{\sum \frac{\boldsymbol{Y_i}}{\boldsymbol{T_{G,i}}}} \qquad (17)$$

In order to be able to spray dry any formulation consisting of any number of components, equations 16 or 17 must be used to calculate the glass transition temperature of each component separately using their dry T_G (known from the literature), the target outlet relative humidity of the spray dryer, and their vapor sorption behavior. The water content should be treated as a second component in order to calculate the T_G in the outlet RH. The glass transition temperature can change with water content. Any material e.g. water that can decrease the glass transition temperature is called a plasticizer [21, 22]. The vapor sorption behavior of a material determines how much water it absorbs in any relative humidity, and the amount of absorbed water determines how much its glass transition temperature changes.

1.3. Mass and Energy Balance in Spray Dryers

In order to predict the spray drying product properties, application of mass and energy balance equations is required [23]. Considering the drying chamber as the control volume (figure 7), there are four terms in the energy balance equation in the most general form [8]:

1) Enthalpy change of the drying gas (ΔH_{dg})
2) Enthalpy change of the atomizing gas (ΔH_{ag})
3) Enthalpy change of the feed solution (ΔH_{sol})
4) Heat loss (H_L)

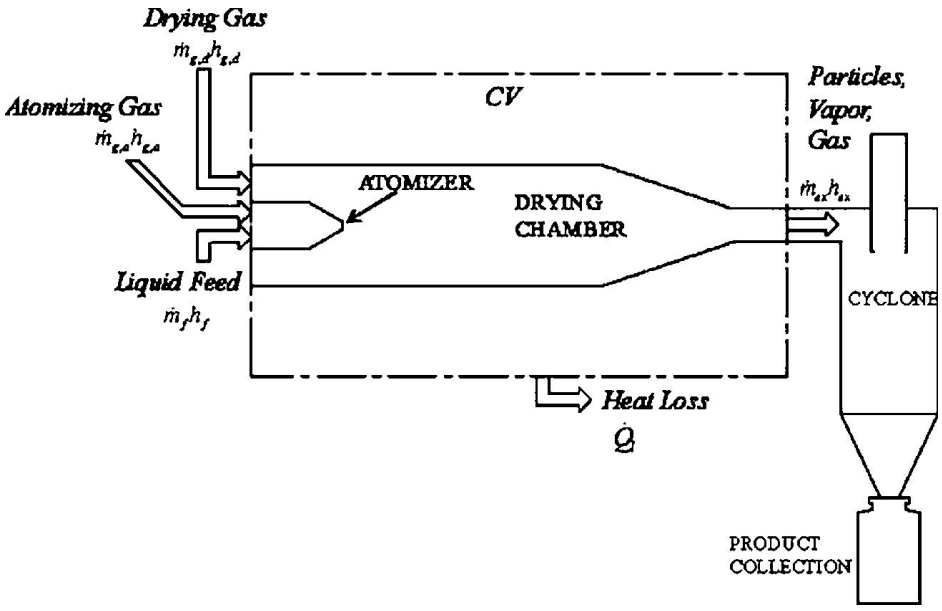

Figure 7 - Drying chamber as the control volume, Reprinted from [24], with permission from Elsevier

Assuming that the drying and atomizing gases are completely dry and there is no pressure change during the drying process, these four terms form the general energy balance equation:

$$\Delta \boldsymbol{H}_{\mathbf{dg}} = \Delta \boldsymbol{H}_{\mathbf{sol}} + \Delta \boldsymbol{H}_{\mathbf{ag}} + \boldsymbol{H}_{\mathbf{L}} \qquad (18)$$

The feed solution consists of water and solid content both of which go through temperature changes. The solid content (x_s) is calculated by dividing the feed concentration by the feed solution density. Since this number is very low in spray drying applications, the enthalpy change of the solid content will be ignored in the following equations.

We assume that drying and atomizing gases with mass flow rates of m_{dg} and m_{ag} enter the drying chamber with T_{in} and T_{feed} temperatures, respectively. The feed solution enters the drying chamber with a mass flow rate of m_{sol} at temperature T_{feed}. The energy provided by the drying gas is used to heat the atomizing gas and vaporize the water content of the feed solution, and they

both reach equilibrium and leave the drying chamber (control volume) at temperature T_{out}.

The energy required to vaporize the water content (or any solvent in a general application) in the feed solution and the enthalpy change of the atomizing gas are shown below [8]:

$$\Delta \boldsymbol{H_{sol}} = \boldsymbol{m_{sol}}(\mathbf{1} - \boldsymbol{x_s})[\boldsymbol{C_s}(\boldsymbol{T_{out}} - \boldsymbol{T_{in}}) + \Delta \boldsymbol{H_{vap}}] \quad (19)$$

$$\Delta \boldsymbol{H_{ag}} = \boldsymbol{m_{ag}}.\boldsymbol{C_{ag}}.(\boldsymbol{T_{out}} - \boldsymbol{T_{feed}}) \quad (20)$$

With C_{s}, ΔH_{vap}, and C_{ag} being the specific heat and the latent heat of evaporation of the solvent, and the specific heat of the atomizing gas. Considering C_{dg} being the drying gas specific heat, the energy supplied by the drying gas is:

$$\Delta \boldsymbol{H_{dg}} = \boldsymbol{m_{dg}}.\boldsymbol{C_{dg}}.(\boldsymbol{T_{in}} - \boldsymbol{T_{out}}) \quad (21)$$

The heat loss can be expressed as a linear function of the outlet temperature [24] as shown in equation below:

$$\boldsymbol{H_L} = \mathbf{A}\boldsymbol{T_{out}} + \mathbf{B} \quad (22)$$

Substituting the last four equations in the general energy balance equation results in:

$$\begin{aligned} \boldsymbol{m_{sol}}.(\mathbf{1} - \boldsymbol{x_s}).\left[\boldsymbol{C_s}(\boldsymbol{T_{out}} - \boldsymbol{T_{in}}) + \Delta \boldsymbol{H_{vap}}\right] \\ + \boldsymbol{m_{ag}}.\boldsymbol{C_{ag}}.(\boldsymbol{T_{out}} - \boldsymbol{T_{feed}}) + \mathbf{A}\boldsymbol{T_{out}} + \mathbf{B} \\ = \boldsymbol{m_{dg}}.\boldsymbol{C_{dg}}.(\boldsymbol{T_{in}} - \boldsymbol{T_{out}}) \end{aligned} \quad (23)$$

Assuming that all specific heats are constant, equation 23 can be re-organized to calculate outlet temperature from inlet parameters:

$$\boldsymbol{T_{out}} = \frac{\boldsymbol{m_{dg}C_{dg}T_{in} + m_{ag}C_{ag}T_{feed} + m_{sol}(1-x_s)\left[C_sT_{feed} - \Delta H_{vap}\right] - B}}{\boldsymbol{m_{ag}C_{ag} + m_{dg}C_{dg} + m_{sol}(1-x_s)C_s + A}} \quad (24)$$

In the general case, a moisture balance equation is required as well [8]. However, in this case, assuming both drying and atomizing gases are completely dry, and ignoring the moisture content of the solid product, leads to a simple equation for the prediction of the outlet relative humidity [23]:

$$\%\mathbf{RH_{out}} = \mathbf{100}.\left(\frac{\boldsymbol{P_{chamber}}}{\boldsymbol{P^*_{T_{out}}}}\right).\frac{\boldsymbol{m_{sol}}.\boldsymbol{(1-x_s)/M_{sol}}}{\boldsymbol{m_{sol}}.\frac{\boldsymbol{1-x_s}}{\boldsymbol{M_{sol}}} + \frac{\boldsymbol{m_{dg}}}{\boldsymbol{M_{dg}}} + \frac{\boldsymbol{m_{ag}}}{\boldsymbol{M_{ag}}}} \quad (25)$$

In which P_{chamber} is the absolute pressure in the drying chamber, $P^*_{T_{out}}$ is the solvent saturation vapor pressure at the temperature T_{out}, M_{sol}, M_{dg}, and M_{ag} are the molecular weights of the feed solution, drying gas, and atomizing gas respectively.

1.4. Applying the Theory to Particle Design

The theory discussed in the previous sections can be used in several consecutive steps to avoid trial and error in the particle design process. This theory leads to a time- and cost-effective approach for spray drying. The general way of application of the theory and order of steps to be taken is demonstrated in the block diagram in figure 8.

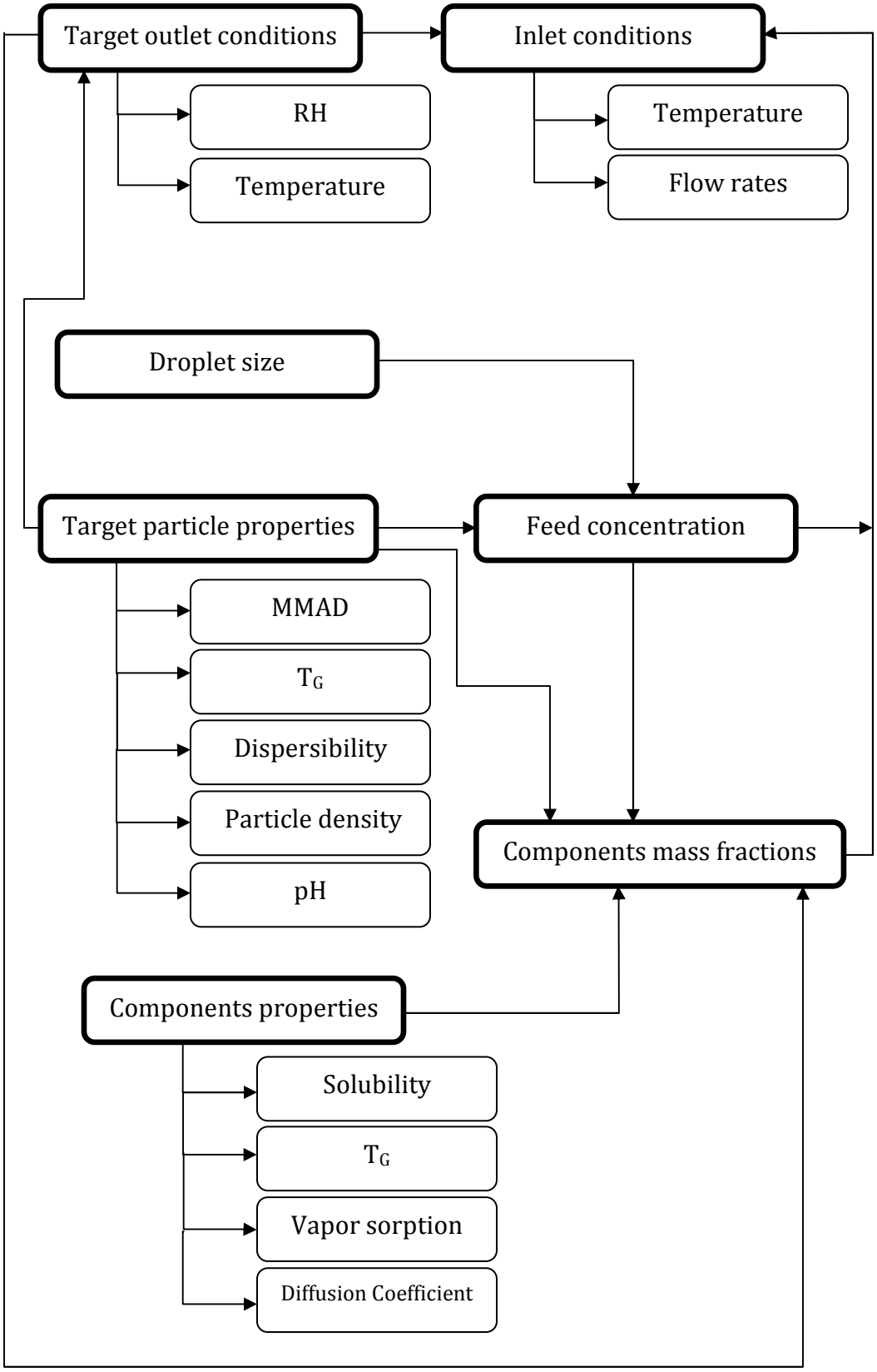

Figure 8 - Particle design for spray drying

Here is a brief explanation of the block diagram:

Droplet diameter, which is a known parameter as one of the specifications of the atomizer used in the spray dryer (might not be fixed in some types of atomizers e.g. twin-fluid), along with the target aerodynamic diameter and particle density, is used to calculate the required feed concentration for spray drying using equation 9.

Target particle properties also determine the outlet conditions for the spray drying process. For instance, low outlet temperature is required to avoid chemical degradation of the components, and low outlet RH prevents particles from plasticization and diffusing together. Other information such as the inhalation device specifications can be taken into consideration when determining the outlet conditions.

Having determined outlet temperature and RH, component's vapor sorption and plasticization behavior can be predicted. The glass transition temperature of all components in outlet conditions can be calculated and used to determine their mass fractions in order to achieve stability goals for the final product. One should note that some of the components' properties such as solubility and pH can pose limitations on their mass fractions. Moreover, calculating Peclet number of the components helps predict the particle formation mechanism and morphology and affects the particle design strategy.

The final step is to determine the inlet conditions of the spray drying process using the information gathered in previous steps. The mathematical model discussed in section 1.3 can be used to determine proper inlet conditions to result in the target outlet conditions using the feed concentration and mass fractions of the components along with thermal properties of the material involved such as drying and atomizing gases.

This methodology will be used in upcoming chapters to engineer pharmaceutical particles for respiratory delivery.

2. Spray Drying of Bacteriophages

2.1. Introduction

Bacterial infections have been treated by chemical antibiotics for decades. However, many types of bacteria, referred to as "superbugs", have become resistant to most available antimicrobials due to genetic mutation [25]. This phenomenon has been observed in several bacterial infections [26–28] among which are bacterial pneumonia and cystic fibrosis. *Burkholderia cepacia* complex and *pseudomonas aeruginosa* are two types of bacteria affecting the lungs of cystic fibrosis patients. These two bacteria strains have developed resistance to a wide range of antibiotics [26, 27].

Considering the casualties caused by bacterial infections and the emergence of antibiotic-resistant bacteria, finding alternative treatments needs urgent attention. Bacteriophage therapy [29–32] could be a good solution. Bacteriophages are viruses that attack and infect bacteria. Figure 9 shows a schematic of the general structure of a bacteriophage. Phages cannot reproduce on their own; they need a host: a bacterium. They use their tail fibers to attach themselves to the host and transfer their DNA from the head into the bacterium. The newly formed bacteriophages will later destroy the bacterium wall, be released to the outside, and each attack a new bacterium. This is the basis of phage therapy [29].

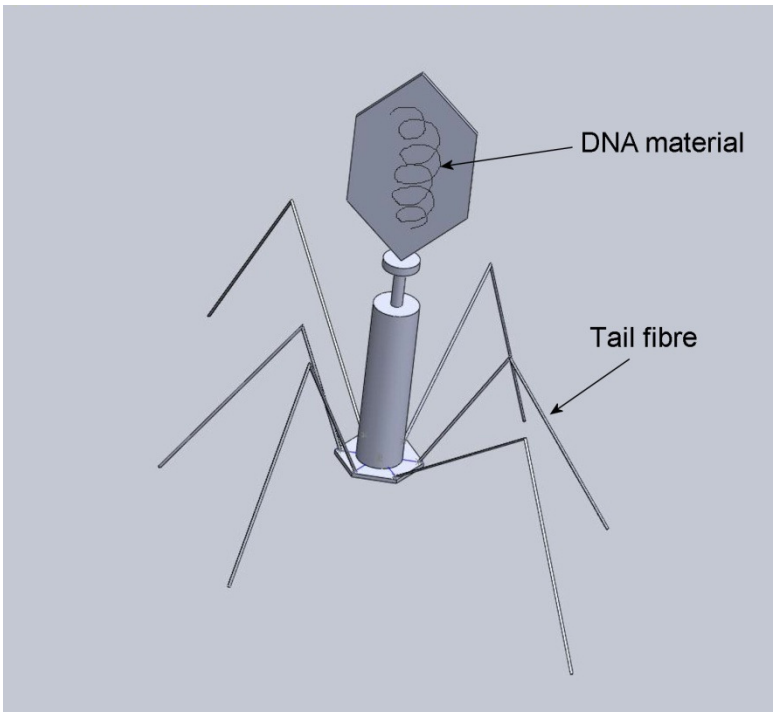

Figure 9 - General phage structure, inspired by [33]

Following is a summary of the information described in existing literature on bacteriophage therapy [34].

Phage therapy has numerous advantages over chemical antibiotics. First and most importantly, each phage infects only a specific type of bacteria. Phages do not affect any of the human cells or the useful bacteria that live in the human body; in fact, we constantly ingest bacteriophages, and there are no side effects such as diarrhoea that can occur in treatment with antibiotics. Moreover, phage therapy is a dynamic and intelligent type of infection treatment since phages only reproduce as long as there are harmful bacteria left to be killed, and they deteriorate after the infection is treated. Furthermore, there is more than one type of phage active against each bacterium, and even if a bacterium develops resistance against antibiotics and specific types of phages, other phages exist in the nature waiting to be found that can treat that bacterial infection [35].

Despite all the advantages of bacteriophages over antibiotics, phage therapy has a number of drawbacks too. To mention a few, the specificity of phages can become an issue when the type of the bacterium causing the infection is not known or where there is a number of bacteria involved. Moreover, phages are harder to administer since they are more complex and larger than chemical molecules [35].

Phages were discovered in early 20th century and tried for medical purposes first on chickens and soon after on humans. Results showed profound success in treating bacterial infections but whether it was due to phages was unknown. Hence, after the invention of penicillin in 1940s, phage therapy was abandoned everywhere except for the former Soviet Union and Poland. Details can be found elsewhere [31]. Western scientists later revisited this type of therapy only after the emergence of antibiotic-resistant bacteria.

Bacteriophages have been successfully used to treat respiratory tract bacterial infections before. Respiratory delivery seems to be the most efficient route of delivery to overcome some issues that we face when dealing with lung infections. Researchers have shown that it is possible to deliver enough doses of bacteriophages to the lung via nebulization [36]. However, it is important to be able to stabilize the bacteriophages in dry powder form for distribution purposes. Freeze-drying has been proved to be efficient enough in developing phages in dry powder form. Since phages are susceptible to thermal stress [37], low-temperature manufacturing methods, such as freeze-drying, can be ideal; however, post-manufacturing processes e.g. micronization are needed.

This study investigates the feasibility of encapsulating phages in specifically engineered micro particles via spray-drying. The ability to design the internal structure for the particles, which is the most important advantage of spray-drying method, helps to improve dispersibility of the final product. Spray-dried particles can also be designed in a way that provides protection against

thermal stresses that phages undergo during the manufacturing process. While normal spray-drying process has been proven to deactivate phages to a large extent [38], low-temperature spray-drying may have less effect on phages' viability.

The results presented in this chapter have been published in a peer reviewed journal [39].

2.2. Materials and Methods

2.2.1. Bacteriophages

Bacteriophages KS4-M, active against *Burkholderia cepacia* complex, and φKZ/D3 cocktail, active against *P. aeruginosa*, were used in this study because they have successfully been nebulized or lyophilized [34, 40] and are easy to obtain in high titers. These bacteriophages are assigned to the *Myoviridae* family due to their morphology (figure 10). The other *Myoviridae* bacteriophage used in this study was KS14. Figure 16 shows its size and morphology compared with the other two bacteriophages.

Bacterial host strains were used to grow bacteriophage lysis in plates incubated at 30 °C overnight. Adding sterile water to the plates and putting them on a platform rocker for 4 to 8 hours at 4 °C resulted in supernatant containing bacteriophages, which were pelleted later through centrifugation. The blend was then filter sterilized, passed through an endotoxin removing column, and stored at 4 °C. Further detail can be found elsewhere [39].

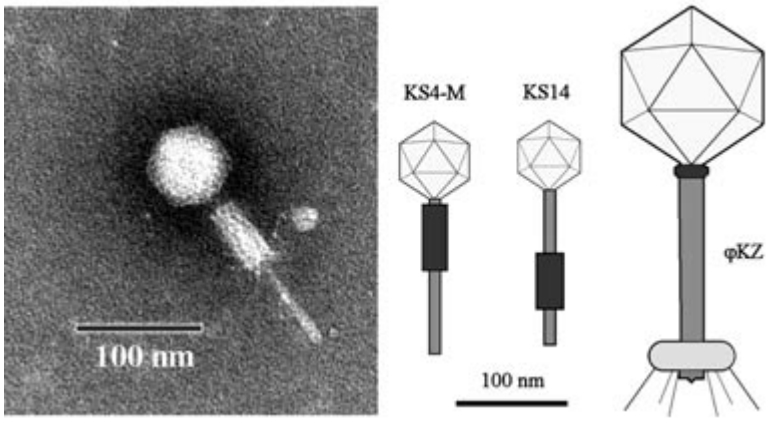

Figure 10 - Schematic of bacteriophages, reprinted from [39], with kind permission from John Wiley and Sons.

2.2.2. Excipients

Trehalose

In order to minimize the bacteriophages' viability loss due to thermal stress and desiccation during the spray drying process [41, 42], α-α trehalose (CAS number 6138-23-4) was used as the main component of each formulation since it has been proven to have low toxicology risk and protect biological material [43, 44]. It also helps increase the final product's shelf-life.

L-leucine

L-leucine was used in all formulations to enhance the dispersibility of the final product from dry powder inhalers. It has been shown that L-leucine reduces the cohesive forces between micro particles [45, 46].

Casein

Casein sodium salt from bovine milk (Sigma–Aldrich, St. Louis, MO) was used in some formulations because it was suspected to have protective effect on

bacteriophages. It has been shown that phages in milk can withstand higher thermal stress than phages in water [47]. The protective effect cannot be due to any fatty components in milk since this effect was also observed in skim milk. Casein, as the main protein in dairy products, is the most probable component that could have caused the protective effect.

Tyloxapol and Pluronic

Surfactants Tyloxapol [4-(1, 1, 3, 3-tetramethylbutyl phenol polymer with formaldehyde and oxirane, CAS number 25301-02- 4] and Pluronic F68 (polyoxyethylene– polyoxypropylene block copolymer, CAS number 9003-11- 6) were added to some formulations to aid in dispersion of bacteriophages in the feed solution.

2.2.3. Formulations

Table 1 shows all the formulations that were spray dried and analyzed. Every formulation mainly consists of trehalose and leucine. LTX and LTP contain surfactants (tyloxapol and pluronic respectively), and LTC contains casein sodium salt. The remaining mass fraction is the bacteriophage solution added to each formulation before spray drying.

Table 1 - Formulations

Formulation Code	LT	LTX	LTP	LTC
Mass fraction, trehalose	0.77	0.76	0.76	0.76
Mass Fraction, leucine	0.19	0.19	0.19	0.19
Mass fraction, surfactant	0	0.02	0.02	0
Mass fraction, casein sodium salt	0	0	0	0.02
Feed concentration (mg/mL)	27	27.5	27.5	27.5

L, T, X, P, and C denote leucine, trehalose, tyloxapol, pluronic, and casein sodium salt

Mass fraction of each excipient was determined using the results from a recent study [48] on spray drying trehalose/leucine formulations for respiratory delivery which suggests that a minimum amount of leucine is required in order to achieve desirable properties in the final product of spray drying.

Figure 11 shows a summary of the findings in the mentioned study. According to these results, a minimum of 30% mass fraction of leucine is required to achieve 100% leucine crystallinity. Leucine mass fraction of 19% was chosen considering 20% leucine mass fraction still results in high crystallinity percent and suitable morphology (fig 11) while providing more trehalose content to protect the biological material and allocating some fraction of the mass to the bacteriophages.

The top right part of the figure shows the surface concentration of L-leucine and trehalose during evaporation of a 25% L-leucine formulation. Leucine must have enough time after saturation to crystallize, and the surface concentration of trehalose at the time when leucine reaches saturation must be low enough to not to interfere with leucine crystallization.

The feed concentration was calculated using equation 8 assuming a target aerodynamic diameter of 2 μm and a droplet diameter of 7 μm (according to Büchi B-90 manual for 4 μm mesh plate discussed in section 2.2.4). The particle density was estimated as a function of leucine mass fraction based on previously published studies on leucine particles [49, 50] and used in this equation.

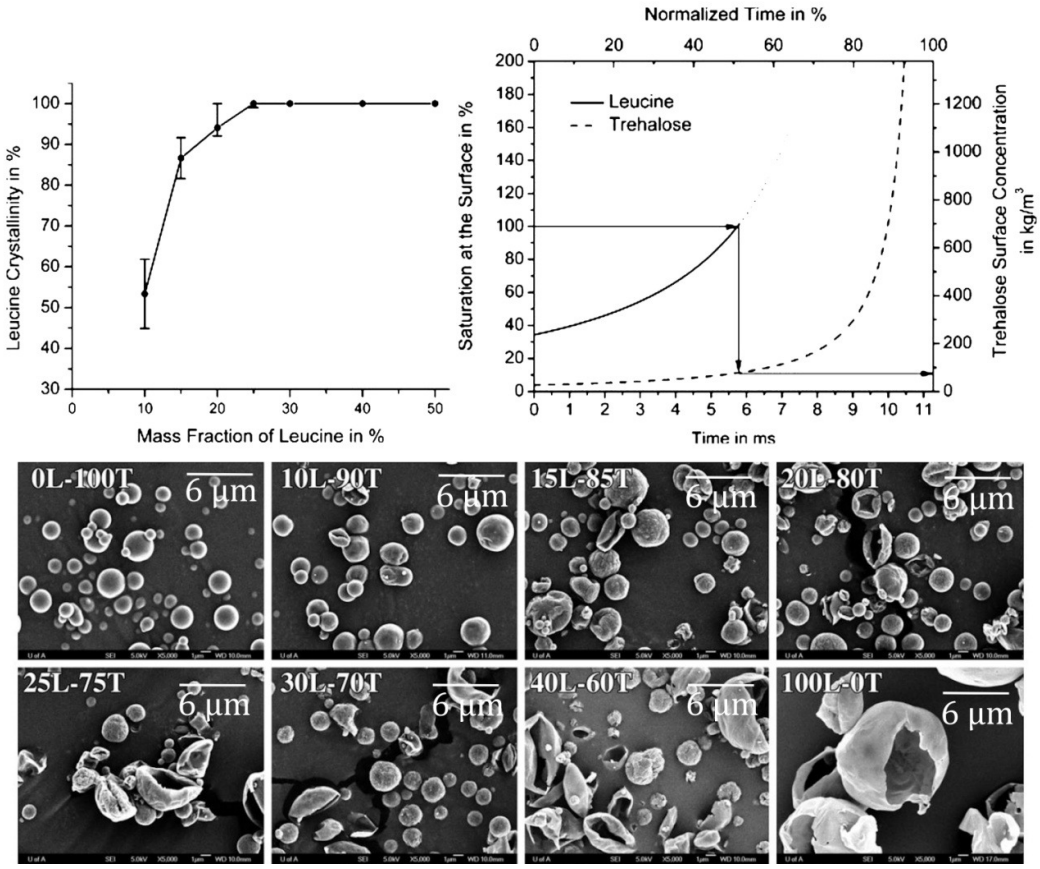

Figure 11 - Leucine crystallinity. Reprinted from [48], with permission from Elsevier

2.2.4. Spray Drying

The spray drying process was performed on a Büchi B-90 laboratory-scale spray dryer. This device produces a fine spray using a vibrating mesh atomizer, which consists of a thin membrane with an array of either of 4, 5.5, or 7 µm holes and is driven by a piezoelectric actuator with ultrasonic frequency, producing droplets in the size range of 3-15 µm. The operating principle of the atomizer is shown in figure 12.

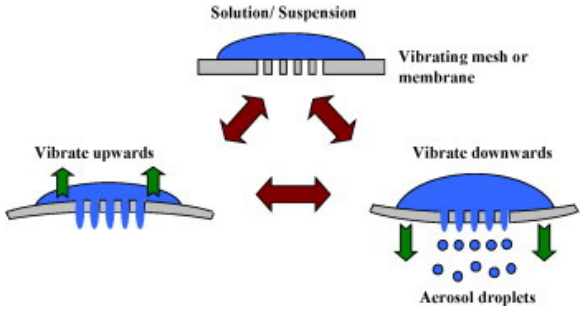

Figure 12 - Büchi B-90 atomizer. Reprinted from [51], with permission from Elsevier.

The spray is then subjected to a laminar drying gas flow in the drying chamber. The laminarity of the drying gas flow is due to the porous metal heater through which it is heated and results in drying times of the order of milliseconds, which makes this spray dryer suitable for drying heat-sensitive material. The solid product is finally collected in an electrostatic particle collector, which is highly efficient in collecting particles of the size range produced in this study, and scraped off the walls of the collector. A schematic of the spray dryer can be seen in figure 13.

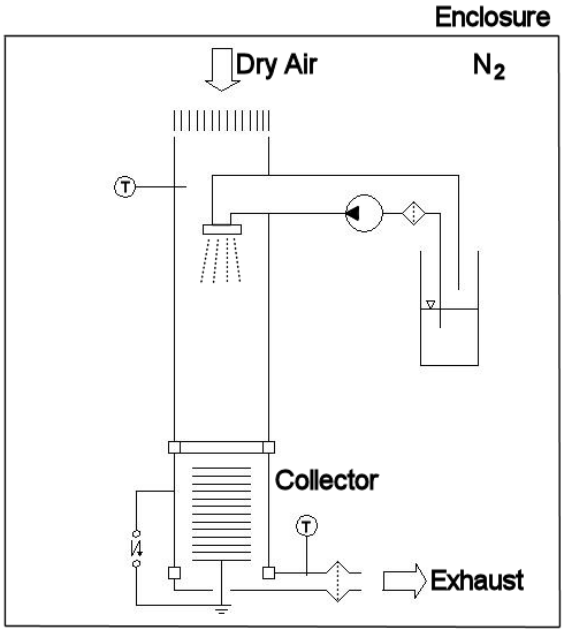

Figure 13 - Schematic of Büchi B-90. Reprinted from [39], with kind permission from John Wiley and Sons.

The Büchi B-90 can spray dry a large variety of materials such as proteins and amino acids with high manufacturing yields using small amounts of liquid; hence, it is suitable for early stages of product development [52]. Figure 14 shows the Büchi B-90 spray dryer standing in a closed box with controlled humidity.

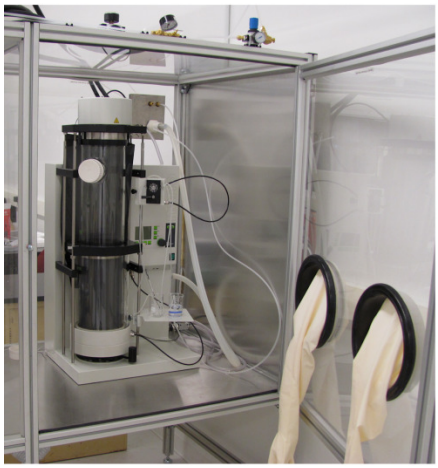

Figure 14 - Büchi B-90 spray dryer

The inlet parameters of the spray drying process were set in order to achieve desirable outlet parameters i.e. low outlet temperature (40-45°C)and relative humidity (<7%). Low outlet RH was required to prevent potential glass transition of the dry product. Low outlet temperature was required to prevent degradation of the excipients. A glove box flushed with Nitrogen was used to keep the RH under 5% throughout the collection process to prevent moisture absorption.

To calculate the heat loss of the spray dryer, several tests were conducted on the spray dryer with only drying gas flowing. The outlet temperature was recorded with varying inlet temperature, and heat loss for each point was calculated using air specific heat. A linear function was then fit through all

data points. A computer model was then developed relating the inlet parameters to outlet parameters using the equations derived in section 1.3 on mass and energy balance in the drying chamber. The inlet parameters were then changed using the model in order to reach desirable outlet temperature and RH. Inlet temperature of 75°C and drying air flow rate of 100L/min returned the target outlet parameters.

2.2.5. Characterisation Tests

Aerosol Performance Test

The aerosol performance of the spray-dried powder was determined by measuring three parameters: emitted mass fraction, mouth-throat mass fraction, and total lung mass fractions. The Aerolizer®, a commercially available dry powder inhaler (DPI), was used along with the Alberta Idealized Throat [40] to determine these parameters. Hard gelatin capsules (#3, Capsule Connections, Prescott, Arizona) were filled with powder doses of 20-30 mg and loaded into the Aerolizer. The DPI was connected to the Alberta Idealized Throat (using a custom fabricated connector) and operated with a flow rate of 60L/min for 4s in each test. Each part of the throat replica was coated with silicone in order to be able to assay the powder deposited in the throat later. A low-resistance Respirgard filter was placed in the outlet of the throat to collect the lung dose mass fraction of the powder. The powder content in throat and the filter were extracted using water and assayed after each test. A plaque assay was also done on the filter extract to determine the efficacious dose of the bacteriophage content. An Anderson cascade impactor was attached to the outlet of the throat replica to determine the aerodynamic particle size distribution of the lung dose mass fraction. The impactor was used with a flow rate of 60 L/min and cutoff aerodynamic diameters of 5.6, 4.3, 3.4, 2.0, 1.1, and 0.51 μm.

Electron Microscopy

Transmission electron micrographs were taken using a Philips/FEI (Morgagni) transmission electron microscope (Department of Biological Sciences, Advanced Microscopy Facility, and University of Alberta). Details can be found elsewhere [39].

Scanning electron micrographs of each sample were taken using a Hitachi SEM S-2500 (Hitachi Ltd., Tokyo, Japan). Samples were put on a carbon tape covered aluminum pin stub and gold-coated to prevent particles from charging during microscopy.

Biological Assay

An aqueous suspension medium was used to dissolve the powder to reach a concentration of 50 mg/mL. The solution was then diluted, plated in soft agar overlays containing the proper host strains, and incubated at 30 °C overnight before the plaques were counted. Details can be found elsewhere [39].

2.3. Results and Discussion

Figure 15 shows the scanning electron micrographs of the four formulations in table 1, from left to right: leucine–trehalose–pluronic (LTP), leucine–trehalose–tyloxapol (LTX), leucine–trehalose (LT), leucine–trehalose–casein (LTC). More than one micrograph was done on each formulation containing different bacteriophages. The small mass fraction of bacteriophages did not have a significant effect on the morphology of the particles. Hence, only four representative micrographs are shown. Particles from all formulations were spherical with internal voids, which make them well-dispersible and suitable for respiratory applications.

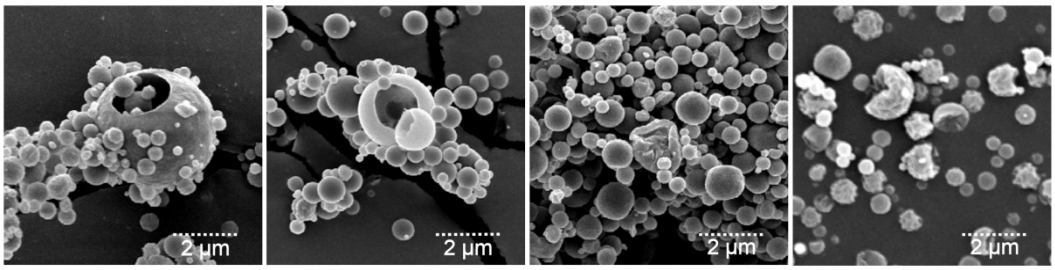

Figure 15 - Scanning electron micrographs. Reprinted from [39], with kind permission from John Wiley and Sons.

Table 2 summarizes the manufacturing yields and aerosol performance results of the four lead formulations. The type of the bacteriophage used with each formulation did not have any significant effect on the results. All of the manufacturing yields listed in table 2 are considered high or acceptable for the small scale in which the study was done. However, one can note that formulations containing surfactants i.e. LTX and LTP had significantly higher yields than the other two.

Table 2 - Aerosol performance

Formulation Code	LT	LTX	LTP	LTC
Manufacturing yield (%)	62.5±5.3§	82.6±5.6§	78.1±4.1§	59.2±3.8*
Emitted mass (% of capsule mass)	NA	82.9±4.7§§	91.7±9.5§	82.7±4.5**
Mouth-throat fraction (% of emitted mass)	NA	28.7±2.8§§	29.3±2.8§	21.8±3.1**

L, T, X, P, and C denote leucine, trehalose, tyloxapol, pluronic, and casein sodium salt, respectively. Error margins refer to a single standard deviation. n denotes the number of replicates.

§n=6, §§n=2, *n=18, **n=8

The emitted mass percent of all the tested formulations were calculated by dividing the sum of the mouth-throat and the total lung powder masses by the capsule powder mass:

$$\textbf{emitted mass}\ (\%\ \textbf{of capsule mass}) = \frac{\textbf{mouth} - \textbf{throat mass} + \textbf{total lung mass}}{\textbf{capsule mass}} \times \mathbf{100} \quad (26)$$

In all of the tests done on the three formulations containing surfactant or casein sodium salt, the emitted dose exceeded 3/4th of the capsule mass, which is higher than all commercially available DPIs [53]. Considering that patients usually exceed the 60 L/min flow rate for the device used here (that was also used in these tests) during inhalation [54], it is likely that the emitted mass of these spray dried powders approaches 100% under typical patient use.

Moreover, data from table 2 shows that almost 70% of the powder emitted from the capsule travels all the way to the lung, and less than 30% of it deposits in the mouth or throat. The powders containing casein sodium salt had significantly higher lung fraction compared with the ones containing surfactant.

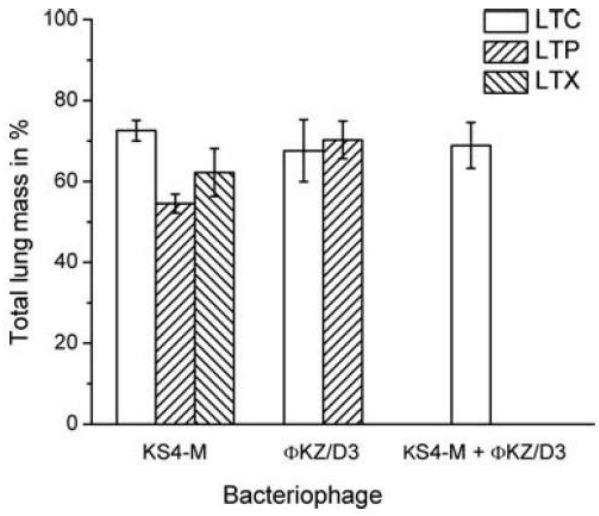

Figure 16 - Total lung mass in % of capsule mass. Reprinted from [39], with kind permission from John Wiley and Sons.

Figure 16 demonstrates the total lung mass in percent of the capsule mass for three different phage combinations in three different formulations for

bacteriophage powders containing KS4-M or φKZ/D3 or a cocktail of phages in different formulations. The formulation codes are explained in Table 1. Error bars represent the standard deviation. While all of the formulations result in higher lung fractions (>50%) compared with the results from commercially available DPIs [53], LTC has the most consistent results for different phages.

Figure 17 shows the particle size distribution of the lung dose fraction for φKZ and KS4-M phages in LTC formulation for two selected bacteriophage formulations in a leucine–trehalose–casein (LTC) formulation. The error bars represent the standard deviation of duplicate tests. The mass median diameters (MMADs) of particles were 2.48 and 2.81 μm for particles containing φKZ/D3 and KS4-M respectively, which is in the size range suitable for respiratory drug delivery i.e. 1-5 μm. There is only a minor difference between the size distributions of the two powders. The increase of the mass percent in the last stage of the impactor is most likely due to particle bounce in the impactor which results in the accumulation of bounced particles of all sizes from previous stages in the final stage.

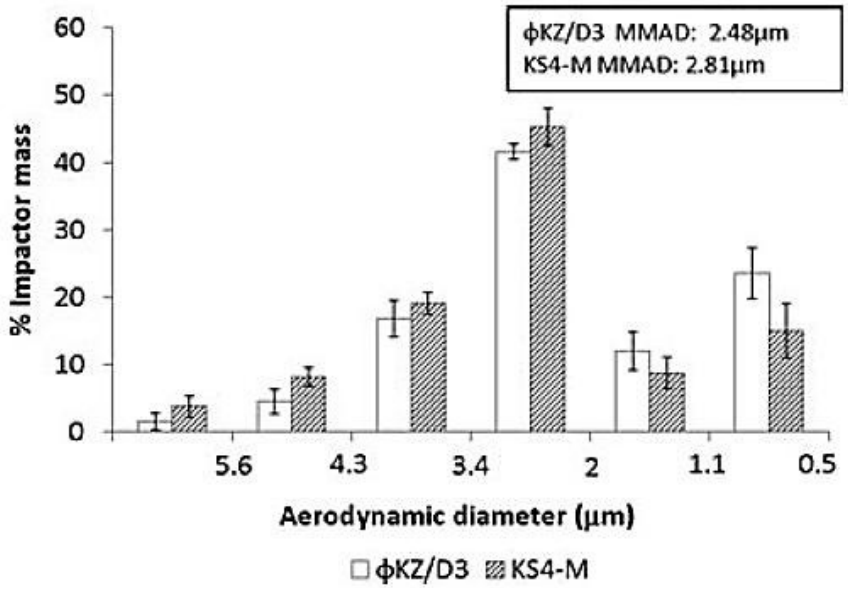

Figure 17 - Aerosol size distribution and MMAD. Reprinted from [39], with kind permission from John Wiley and Sons.

Figure 18 demonstrates the bacteriophages viability loss after the spray drying process both separately and in cocktail using different formulations during the process. The error bars represent the standard deviations. Phages φKZ/D3 and KS4-M were spray-dried and tested in all four formulations. φKZ/D3 phage cocktail was the most resilient to the thermal stress during the process and had less than 0.5 log pfu/mL titer loss irrespective of the formulation. Phage KS4-M had much lower titer loss in LTC than the other three formulations. This led us to repeat the test for other phages as well: KS-14 and a cocktail of φKZ/D3/KS4-M. Results from all the tests show that LTC is the best formulation to preserve the bacteriophages from the stresses they go through during the spray drying process. Titer losses less than 1 log pfu/mL is considered acceptable in terms of manufacturing feasibility.

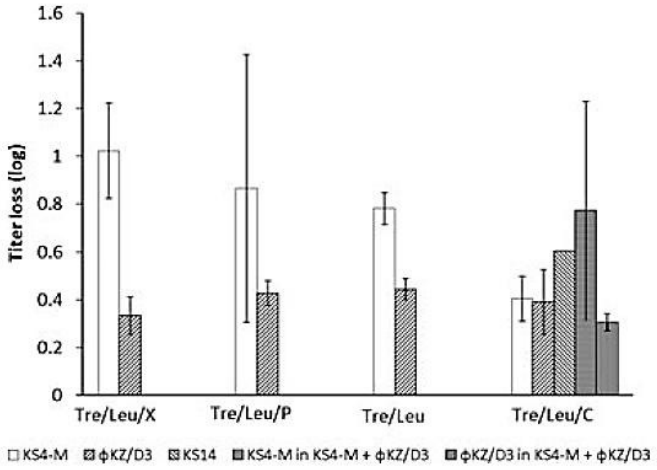

Figure 18 - Titer loss of the phages. Reprinted from [39], with kind permission from John Wiley and Sons.

Figure 19 shows the total lung doses of each phage formulation in pfu. Research has shown a minimum dosage of $3*10^6$ pfu to be efficacious in mice with lethal P. aeruginosa infection [55]. A single dose of $6*10^5$ pfu of phages has been proven to be effective for treatment of ear infection in human caused by P. aeruginosa [56]. Figure 23 shows that the total dose of the bacteriophages delivered to the lungs was likely high enough to be

efficacious. In this figure the diamond represents the median (horizontal line). Vertices show one standard deviation. The whiskers and closed symbols represent the minimum and maximum and mean values.

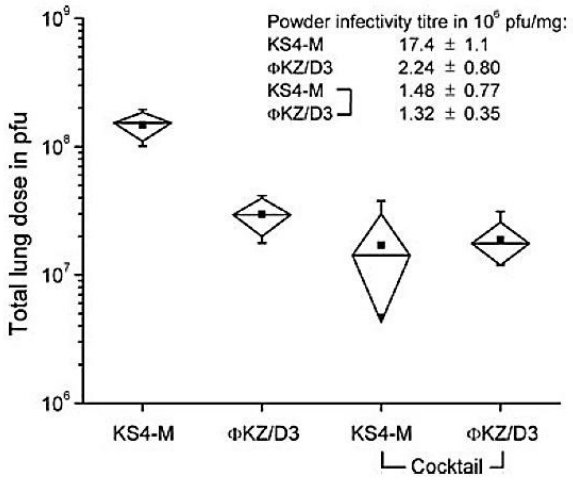

Figure 19 - In vitro total lung dose and powder titer. Reprinted from [39], with kind permission from John Wiley and Sons.

2.4. Conclusions

Bacteriophages can be formulated into dry powder form via low-temperature spray drying. Specific inlet parameters and formulations of low toxicity risk material can be used to develop desirable internal structure for the final micro-particles in order to improve dispersibility and resistance to thermal stress. The final particles had desirable shape (wrinkled spheres with internal voids) and size (mass median aerodynamic diameter of around 2.5 μm for LTC formulation) for respiratory delivery. The manufacturing yield of the process was high enough considering the small batch sizes used for spray drying: a minimum of 55.4% and a maximum of 88.2% for different

formulations. The process loss for all of the bacteriophages in all formulations was less than 1 log pfu/mL, although different for each phage, which is considered acceptable in terms of manufacturability. Powders containing all phages had very high aerosol performance when aerosolized using a commercially available DPI; the emitted mass in percent of the capsule load even reached 100% in some cases. The *in vitro* lung doses delivered from the capsules contained sufficient dosage of phages at a level proved to be efficacious in animals.

3. Spray Drying D-Amino Acids

3.1. Introduction

Bacteria can grow on almost every surface whether industrial or biological. They usually form cell communities –referred to as biofilms- which help them survive by protecting them from their surrounding environment [57–59]. Biofilms, which are observed in 65% of bacterial infections in human [60], can also aid bacteria by keeping them in a dormant state until conditions are more suitable for their growth. Moreover, biofilms make bacteria more difficult to treat since they contain high portions of persister cells, which are in a dormant state and, therefore, very tolerant to antibiotics [61, 62].

Several mechanisms can be employed to form biofilms depending on the bacterium type and its environmental conditions; however, in all biofilms, an extracellular matrix containing polysaccharide biopolymers, extracellular DNA (eDNA), and adhesive proteins are used to hold bacteria together [63].

Pseudomonas aeruginosa bacterial biofilms are often observed in the lungs of cystic fibrosis patients, providing protection against antibiotics and the host's immune system [64–68]. Figure 20 demonstrates (A) biofilm in bronchia of a CF patient treated with several periods of different antibiotics, (B, C) bronchiole filled with bacteria, (D, E) intraluminar biofilms and (F) intact bronchi wall. Although helping to keep maintain the lung's function,

even aggressive antibacterial treatments cannot fully eradicate the bacteria in biofilms [69], and the main effective treatment is to eliminate the bacteria before they form biofilms [70, 71]. Since identifying the disease in its early stages may not always be possible, the need for a treatment for bacteria in biofilms has emerged.

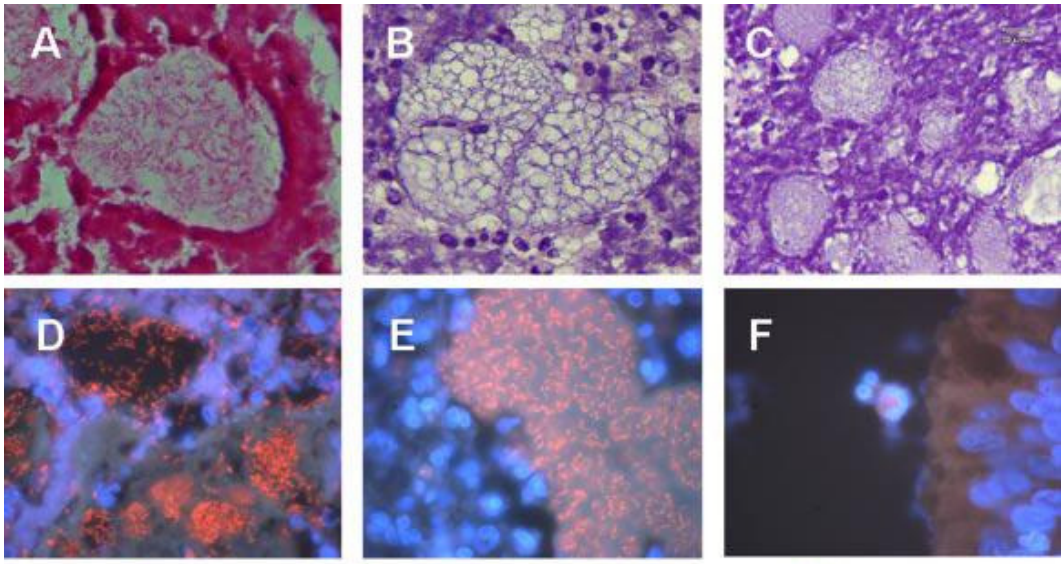

Figure 20 - P-aeruginosa biofilms. Reprinted from [72], with kind permission from John Wiley and Sons

The sputum layer covering the lungs of cystic fibrosis patients provide carbon and energy for *P-aeruginosa* to grow [73, 74]. Research has shown that the amino acids existing in the sputum are also good nutritional sources for *P. aeruginosa* bacteria [74, 75]. Amino acids, which are often referred to as "building blocks of proteins" [76], can exist in many forms. However, the most important amino acids that are found in living organisms are alpha amino acids with the general structure of R-CHNH$_2$(alpha)-COOH where R is a side chain specific to each individual amino acid. In this type of amino acids, both –COOH and –NH$_2$ groups are attached to the same carbon atom [76]. Alpha amino acids are chiral molecules, i.e., they cannot be superimposed on their mirrored image. The terms enantiomers or optical isomers are used to

refer to the two mirror images of any chiral molecules [77]. D- and L-alpha amino acids are the two enantiomers of alpha amino acids (figure 21).

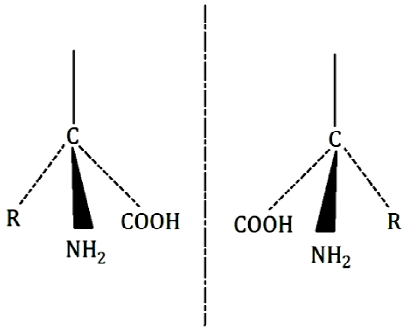

Figure 21 - Amino acid enantiomers, inspired by [78]

L-isomers of alpha amino acids are the ones that naturally exist in living organisms [76]. A recent study demonstrates that seven of 19 L-amino acids found in the CF sputum layer enhance the formation of bacteria biofilms in CF patients [79]. The fact that L-leucine is among these seven amino acids may raise questions about the use of L-leucine as a dispersibility enhancer for respirable therapeutics for cystic fibrosis.

D-amino acids can be found in some food and living organisms [80]. In fact, some bacteria produce D-amino acids in their stationary phase [81]. These D-amino acids will then change the structure of the proteins used to build the cell walls in the bacteria [82]. The observation that bacterial biofilms disassemble after a certain amount of time raised the question whether the D-amino acids produced by the bacteria were a contributing factor [57]. Research showed that a combination of four D amino acids, D-tyrosine, D-methionine, D-tryptophan, and D-leucine of 10 nM each can help disassemble *P. aeruginosa* biofilms [83]. Also, higher concentrations of each of these D-amino acids alone (3 μM D-tyrosine, 2 mM D-methionine, 5 mM D-

tryptophan, and 8.5 mM D-leucine) were shown to be effective [57]. Figure 22 demonstrates how treatment by 100 mg/L^{-1} D-tyrosine helped disassemble biofilms on a membrane. The pre-cultured biofilm is shown before (left) and after (right) the treatment.

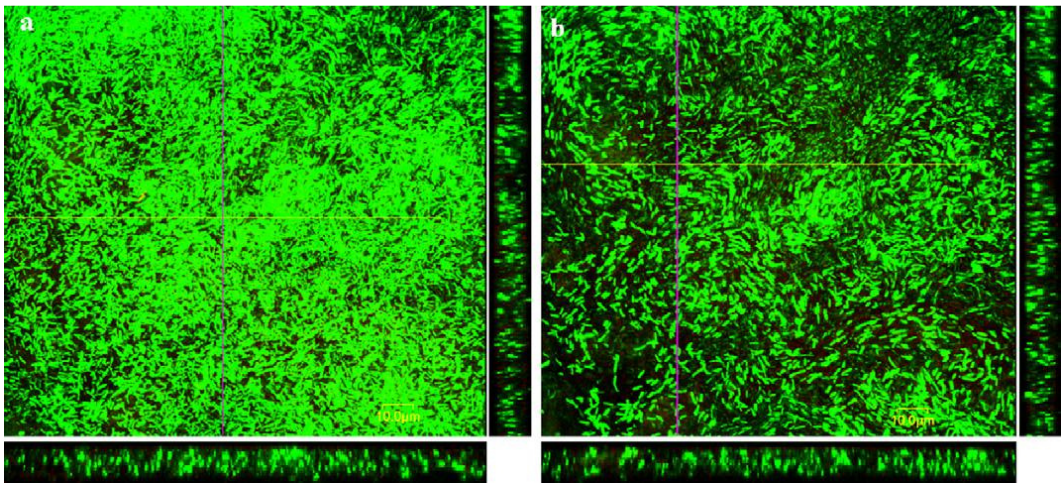

Figure 22 - Biofilm disassembly. Reprinted from [82], with permission from Elsevier

Considering that L-leucine, a common dispersibility enhancer, contributes to *P. aeruginosa* biofilm growth [79] while D-leucine helps disassemble them, this study mainly investigates the feasibility of substituting L-leucine with D-leucine in aqueous formulations for spray drying. Since D- and L- isomers have nearly identical physical properties, D-leucine was spray dried using the same approach used earlier for spray drying L-leucine-containing solutions. It is essential that the final product containing D-leucine has as good an aerosol performance as the dry powders containing L-leucine. We also added D-methionine to some formulations in order to further investigate the feasibility of developing dry powder containing all four D-amino acids that have been proven to be effective against *P. aeruginosa* biofilms in CF patients. Several characterization tests were done on each powder to assess whether the final products are suitable for pulmonary delivery.

3.2. Materials and Methods

3.2.1. Amino Acids

L-leucine (CAS number 61-90-5) from Acros Organics and D-leucine (CAS number 328-38-1) from Sigma Aldrich were used in aqueous formulations. The mass fractions of each amino acid, as can be seen in table 4, were determined based on the information provided in the previous chapter.

D-methionine (CAS number 348-67-4) from Sigma Aldrich was added to some formulations as the first step to investigate the feasibility of spray drying the combination of the four D-amino acid discussed before, the properties of which can be found in the table 3 [84].

Table 3 - Properties of the discussed D-amino acids

D-amino acid type	D-Leu	D-Tyr	D-Trp	D-Met
Solubility (mg/mL)	20	0.45	10	30
Melting point (°C)	293	300	282-285	136
Boiling point (°C)	---	351	---	278
Molecular weight (g/mol)	131.173	181.189	204.23	149.211
True Density (g/cm^3)	1.293	---	---	1.206

3.2.2. Excipients

Trehalose (CAS number 6138-23-4) from Fisher BioReagents was used in all formulations due to its successful performance in previous studies as a protective agent [39]. Details can be found in the previous chapter.

3.2.3. Formulations

L-leucine, D-leucine, and D-methionine were spray dried in aqueous solutions containing trehalose. Mass fractions of each material in all formulations are listed in table 4. These mass fractions were calculated using the model discussed in the introduction chapter to achieve high aerosol performance. T, L, D, and M denote trehalose, L-leucine, D-leucine, and D-methionine respectively.

Table 4 – Formulations

Formulation	TL	TD	TDM
Mass fraction, trehalose	0.8	0.8	0.8
Mass fraction, L-leucine	0.2	NA	NA
Mass fraction, D-leucine	NA	0.2	0.1
Mass fraction, D-methionine	NA	NA	0.1

3.2.4. Spray Drying

The Büchi B-90 spray dryer was used to develop dry powder from each formulation. Refer to the previous chapter for details on the spray dryer and process conditions. In summary, each sample solution was spray dried for one hour with an inlet temperature of 75 °C and drying gas flow rate of 100 L/min.

3.2.5. Characterization Tests

Scanning Electron Microscopy

Small amounts of each sample powder were put on a carbon-tape covered aluminum pin stub and gold-coated to prevent charging of the particles throughout the imaging process. Cautions were taken to protect particles from absorbing humidity, which could fuse them together and affect the results of the study: samples were prepared in a glove box with 0% relative humidity and kept in a desiccators cabinet -until carried to the testing area in closed containers with desiccants. Then, high-resolution images of the structure and surface texture of the micro-particles were taken at several magnifications from 500x to 10,000x using a JEOL 6301F field emission scanning electron microscope.

Density Measurement

Compressed bulk density (CBD) of each powder sample was measured using the University of Alberta Density Tester [85]. This device was developed in the particle engineering group of University of Alberta to measure the bulk density of pharmaceutical dry powders under a range of pressures and controlled temperature and relative humidity, which is important to prevent any changes in densification behavior of the sample. The University of Alberta Density Tester needs less than 0.15 cm^3 of powder, which makes it suitable for characterisation tests in the early stages of drug development. The pressure on a known mass of powder in a small cavity increases by an automatic actuator controlled with NI Lab view. The collected data is processed into a density vs. pressure graph. Figure 23 shows a picture of the device.

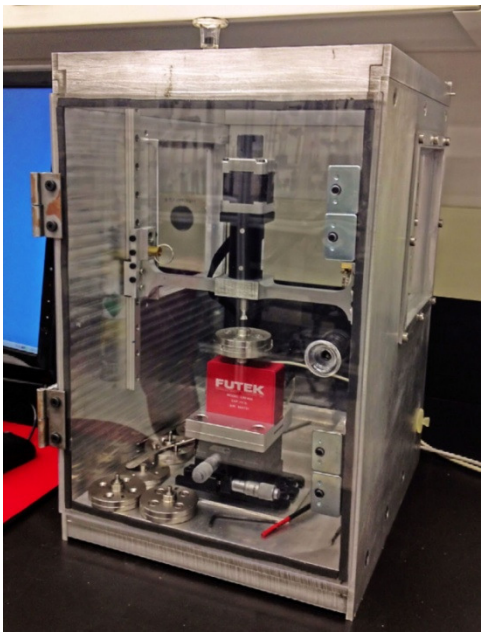

Figure 23 - UAlberta Density Tester

Raman Spectroscopy

A custom Raman system developed in the particle engineering group of University of Alberta [86] was used to analyze the solid state of each sample. Operating with very small amounts of powder i.e. <1.5mg and under controlled temperature (21±1˚C) and relative humidity (<5%), the crystalline and amorphous content of the powder samples were determined using this device. Details of the methodology used in the system can be found elsewhere [86].

Modulated Differential Scanning Calorimetry

To further investigate the crystalline and amorphous content of the powders and the glass transition temperature of the components, modulated differential scanning calorimetry was done on each powder sample using a TA Instrument Q1000 differential scanning calorimeter. Standard aluminum pans with four pinholes in the lids were filled with ~4 mg of powder, and

then equilibrated and kept isothermal at 20°C for 30 minutes. Samples were then heated to ~20°C above T_G at a rate of 10°C/min and rapidly cooled down at a rate of 20°C/min to evaporate the water content and reduce the enthalpic relaxation endotherm. Samples were again equilibrated and kept isothermal at 20°C for 30 minutes, and then heated to a high temperature. The mDSC conditions for each test can be found in tables 5 and 6. T, M, L, and D denote trehalose, D-methionine, L-leucine, and D-leucine respectively.

Table 5 - mDSC methodology

Sample	T	TL_1	TL_2	TD
1st equilibration temp. (°C)	20	20	10	20
1st isothermal time (min)	30	20	30	20
1st heating high temp. (°C)	150	130	130	NA
1st heating Rate (°C/min)	10	10	10	NA
Cooling low temp. (°C)	20	20	20	NA
Cooling rate (°C/min)	20	20	10	NA
2nd equilibration temp. (°C)	20	20	10	NA
Modulation (every 60s)	NA	±0.318°C	±0.08°C	±0.318°C
2nd isothermal time (min)	30	20	30	20
2nd heating high temp. (°C)	250	250	180	250
2nd heating rate (°C/min)	10	2	0.5	2

Table 6 - mDSC methodology for formulations containing D-methionine

Sample	M	TM_1	TM_2	TDM
Equilibration temp. (°C)	20	20	20	20
Equilibration time (min)	20	20	20	20
Modulation (every 60s)	±0.318°C	±0.318°C	±0.318°C	±0.318°C
Isothermal time (min)	20	20	20	20
Heating high temp. (°C)	270	250	180	180
Heating rate (°C/min)	2	2	2	2

Aerosol Performance Tests

The aerosol performance of each spray-dried powder was determined in the same way described in the previous chapter: emitted mass fraction, mouth-throat mass fraction, and total lung mass fraction were measured using the Aerolizer® along with the Alberta Idealized Throat. Gelatin capsules, as described before, were filled with powder doses of 20 mg containing D-amino acids and loaded into the Aerolizer®. The DPI was then connected to the silicone-covered Alberta Idealized Throat and operated with a flow rate of 60 L/min for 4s in each test with the filter connected to the outlet of the throat. The only modification made in this study was putting the whole assembly in an environmental chamber with constant temperature of 25 °C and relative humidity of 30%.

The powder content in throat and the filter were extracted using water and assayed for amino acid content after each test.

Size Measurement

Each powder sample was tested on a TSI Aerodynamic Particle Sizer® (APS) in combination with a Small Scale Powder Dispenser (SSPD). The Small-Scale Powder Disperser was used to generate the aerosol and convey it to the APS for particle sizing. Following, is a brief explanation of how this device works. A stepper motor turns a circular turntable. There is a round abrasive paper with three rings of different radii glued to the turntable. For each test, a small amount of the powder sample was put to the outer ring of the abrasive paper using a brush provided with the device. The stainless steel capillary tube just above the turntable aspirates the powder particles from the surface and conveys them into the venturi throat as a result of the filtered dry air flowing into the venturi at high pressure. Shear forces due to the velocity difference in the capillary tube and the venturi throat deagglomerate the particles

entering the APS which must be located on top of the disperser. The unused powder is filtered and the filtered air exhausted.

This device can disperse aerosols with particle size range of 1 to 50 μm aerodynamic diameter. It cannot deagglomerate particles smaller than 1μm efficiently. We knew from previous studies that the approximate aerodynamic diameter of the particles in our powder samples is 2-3 μm. The range of rotation speed for the turntable was 0.25 to 3.3 rev/hour either clockwise or counter clockwise.

The Aerodynamic Particle Sizer® uses a time-of-flight technique to measure the aerodynamic diameter of particles in the range of 0.5 to 20 μm real-time. The custom optical system used in the APS allows the device to detect and differentiate particles entering the detection area simultaneously, which results in more accurate size measurement. This is how this device works: The particles are accelerated in the nozzle depending on its aerodynamic diameter: the larger the particle, the lower its acceleration. The light scattered by each particle is collected, focused, and converted to an electric signal. Each particle in the measurement range generates a signal with two crests the peak-to-peak distance of which determines the aerodynamic diameter.

3.3. Results and Discussion

The scanning electron microscopy showed that all formulations containing L- or D-amino acids had proper morphology for pulmonary drug delivery. Figure 24 demonstrates the morphology of trehalose (upper left), trehalose/L-leucine (upper right), trehalose/D-leucine (lower right), and trehalose/D-leucine/D-methionine (lower left) formulations. The images shown in this figure are only representatives of multiple images that were taken from each sample in three different magnitudes. Particles containing

one or both L- and D-amino acids had hollow and wrinkled structure, while the samples containing only spray dried trehalose were composed of solid spheres. This can be explained by the particle formation theory described in section 1.2. The L- or D-leucine content of the droplets reaches saturation on the surface of the droplets much sooner than trehalose considering that Peclet number is higher than 1 for leucine and lower than 1 for trehalose. With low trehalose concentration at the surface and enough time for leucine to crystallize, a leucine shell forms and results in hollow and wrinkled particles. Pure trehalose, however, forms solid spheres since the solid content redistributes evenly throughout the droplet evaporation process and does not form a shell. As explained in previous chapters, solid particles do not have good aerosol performance.

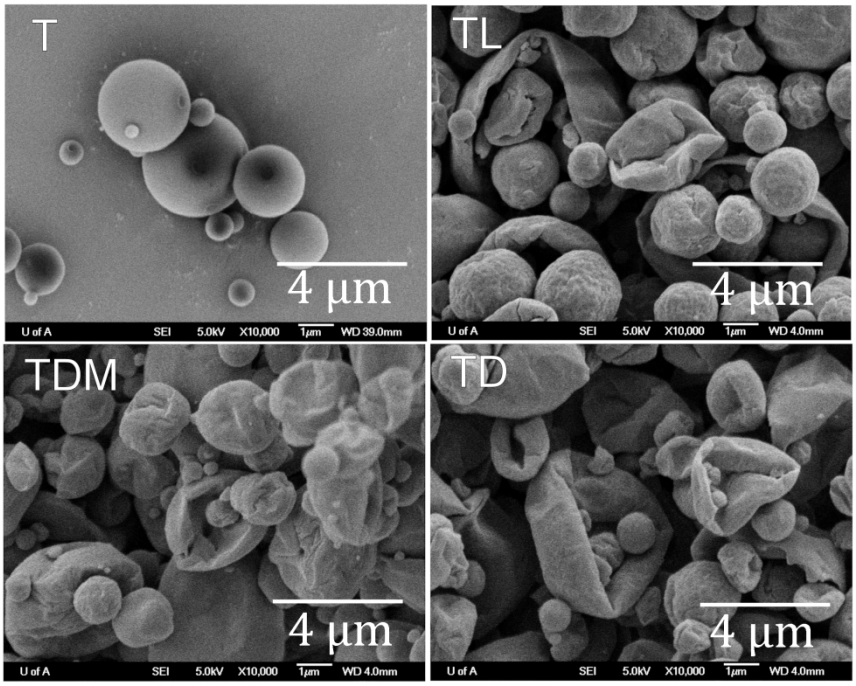

Figure 24 - Morphology of the spray-dried formulations

The density measurements were done on trehalose/L-leucine and trehalose/D-leucine formulations for a range of pressures. The results, which can be seen in figure 25, showed that the two spray dried samples had very

similar densities: 725.6 kg/m^3 for trehalose/D-leucine and 704.8 kg/m^3 for trehalose/L-leucine under 35 kPa pressure, the pressure at which the powder is compressed enough to reveal the compressed bulk density without breaking the individual particles and compromising their true density. The similar compressed bulk density implies that the aerosol performance of the two powders can be similar as well.

This method of density testing has the advantage of applicability to small powder samples. Tapped density testing is another technique to measure the powder bulk density but it requires large amounts of powder. Moreover, in the scale of pharmaceutical particles, inter-particle forces interfere gravity which is the basic concept behind tapped density testing.

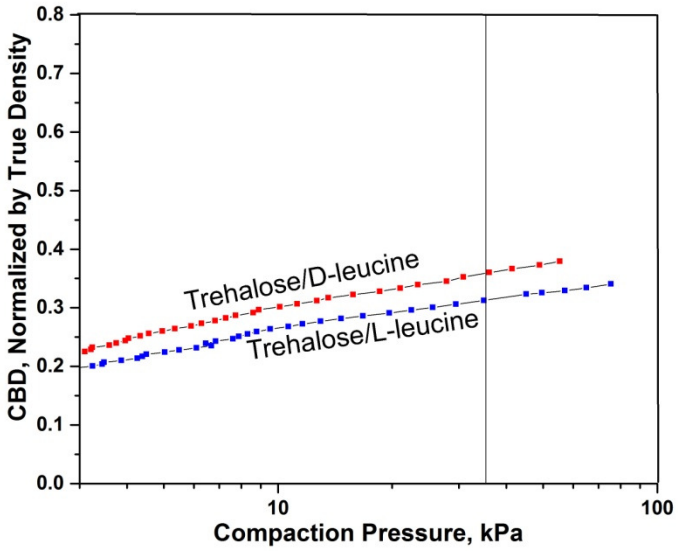

Figure 25 - Compressed bulk density of TL and TD formulations

Raman spectroscopy showed crystalline L- and D-leucine and amorphous trehalose content in the powders as expected.

Figure 26 (top) demonstrates the results from Raman spectroscopy on the raw (crystalline) L- and D-leucine. The spectra are very similar for the two materials. The bottom part demonstrates the Raman spectra for the L- and D-leucine content of the spray dried L- and D-leucine/trehalose formulations. This was achieved by subtracting the spectra for amorphous trehalose from the spectra of the powder samples. The matching peaks of the subtracted spectra and the spectra from raw materials suggest that the D- and L-leucine content of the powder samples are crystalline. This was expected since leucine reaches surface saturation early enough in the droplet evaporation process to have enough time to crystallize.

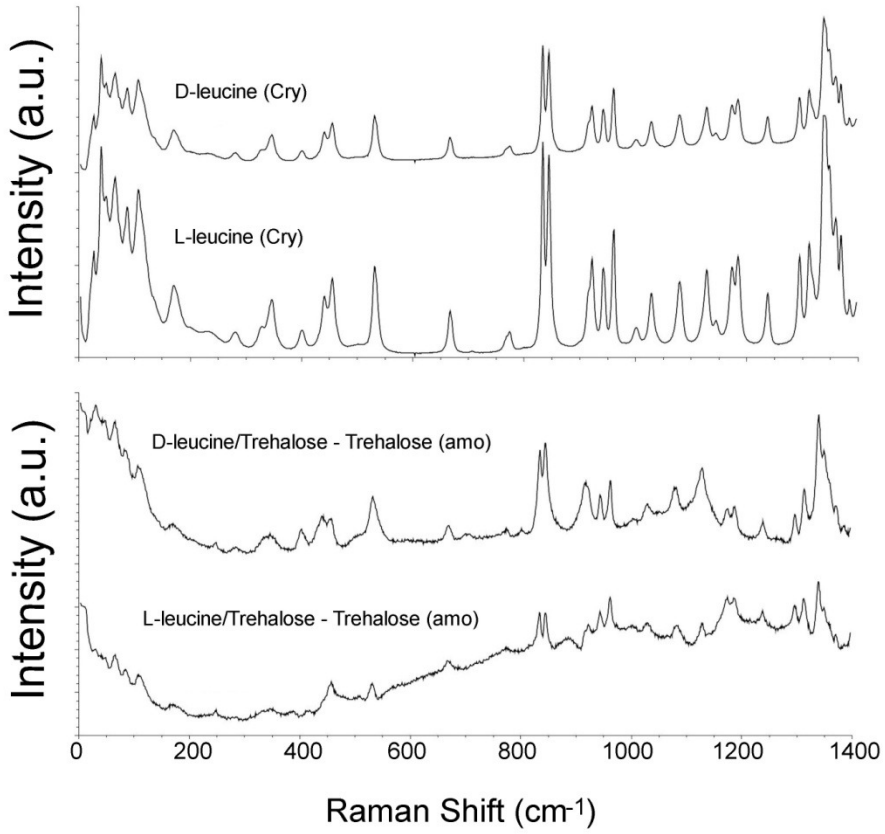

Figure 26 - Raman spectroscopy results for L- and D-leucine

Figure 27 demonstrates that the D-methionine content of the spray dried trehalose-D-methionine is crystalline since the Raman spectra peaks matches the ones from raw crystalline D-methionine.

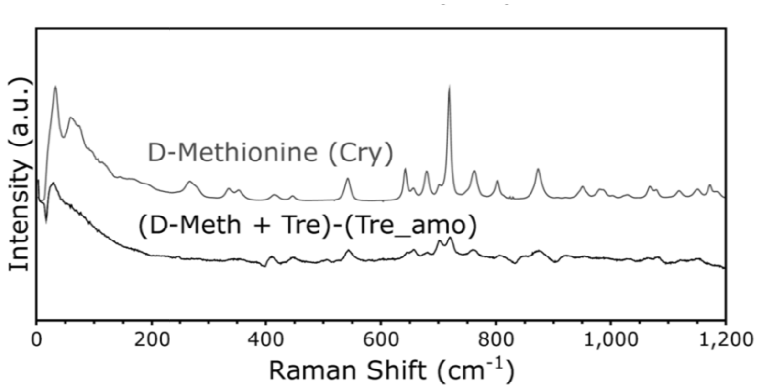

Figure 27 - Raman spectroscopy results

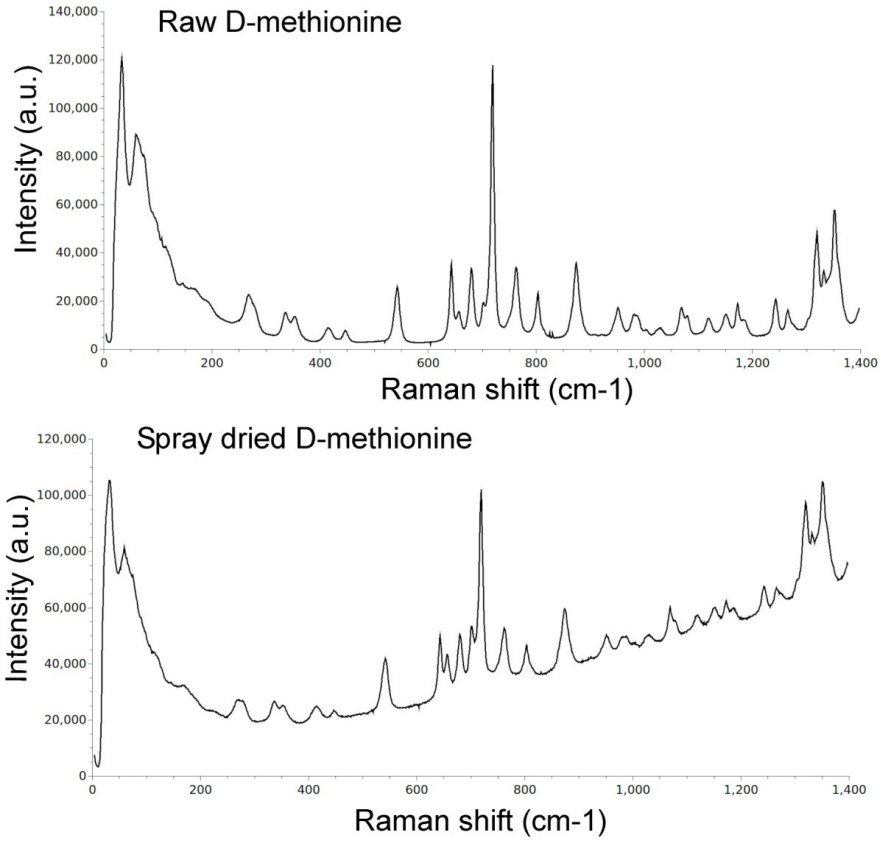

Figure 28 - Raman results for spray dried D-methionine

Figure 28 demonstrates Raman spectra of raw and spray dried D-methionine. Comparing the peaks of the spectra results in the conclusion that spray dried D-methionine is not the same state as raw D-methionine i.e. crystalline and is partly amorphous.

The DSC run on spray dried trehalose (figure 29) showed an endothermic change in the heat flow which corresponds to a glass transition at 119.8C. This number matches the glass transition temperature reported for trehalose in literature [87, 88]. This illustrates that spray dried trehalose is in amorphous state and undergoes glass transition when heated.

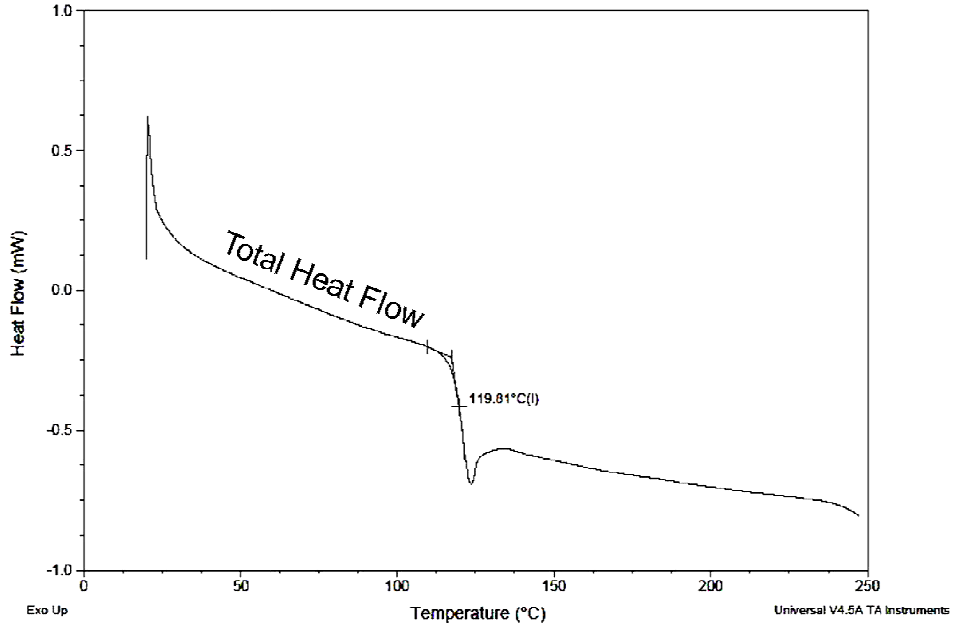

Figure 29 - DSC result for spray dried trehalose

Figure 30 demonstrates the result from modulated DSC on two samples of spray dried trehalose/L-leucine. Endothermic changes seen in the reversing heat flow charts in both tests show glass transition temperatures of around 119 C for both samples while non-reversing endothermic changes

correspond to enthalpic relaxation: the process of a non-equilibrium glassy system approaching to equilibrium which results in change in the thermodynamic properties of the system e.g. enthalpy [89].

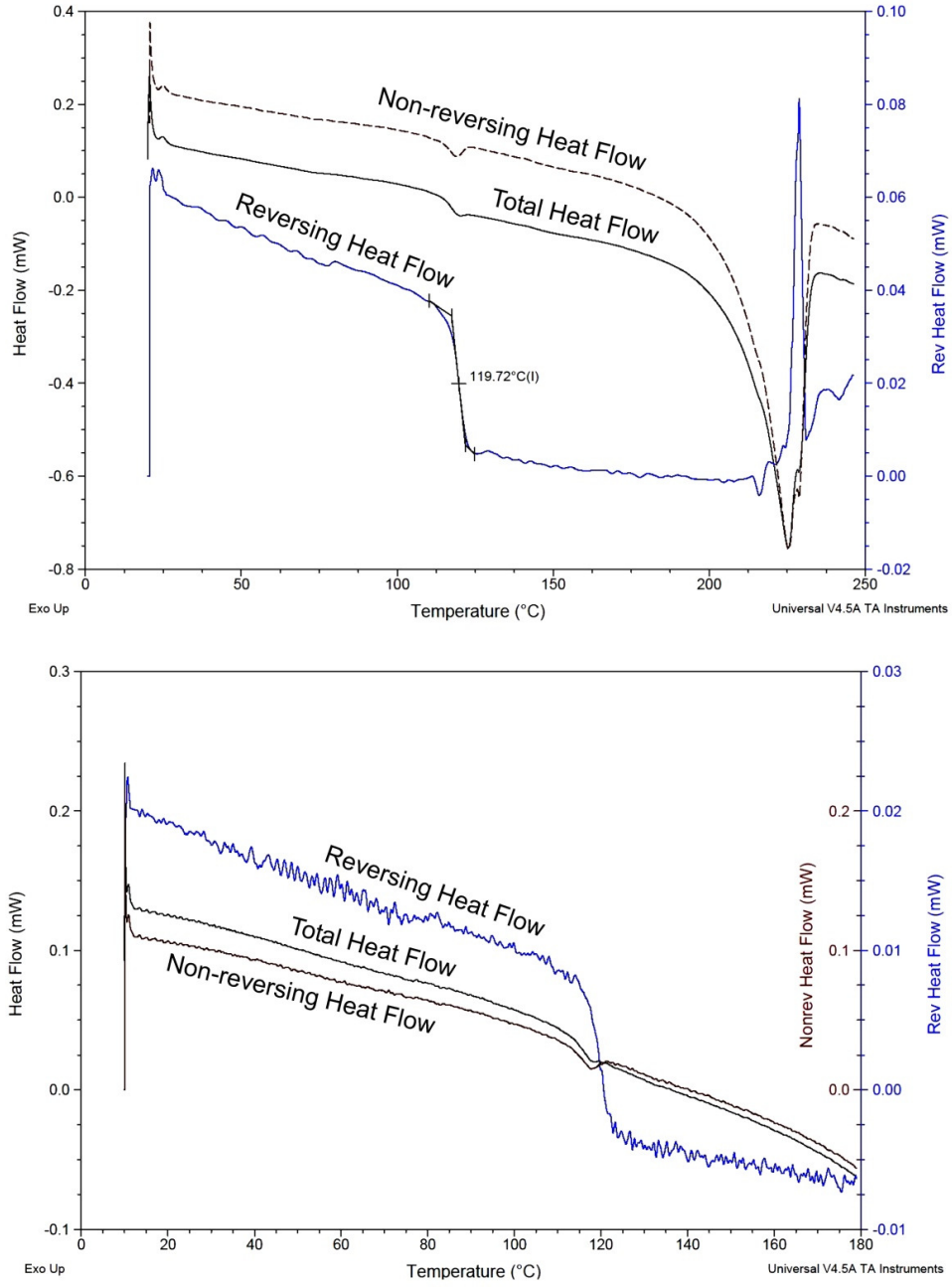

Figure 30 - mDSC results for trehalose/L-leucine

Modulated DSC on spray dried D-methionine did not show any glass transition temperature (figure 31) indicating that D-methionine was all crystalline in the spray dried particles.

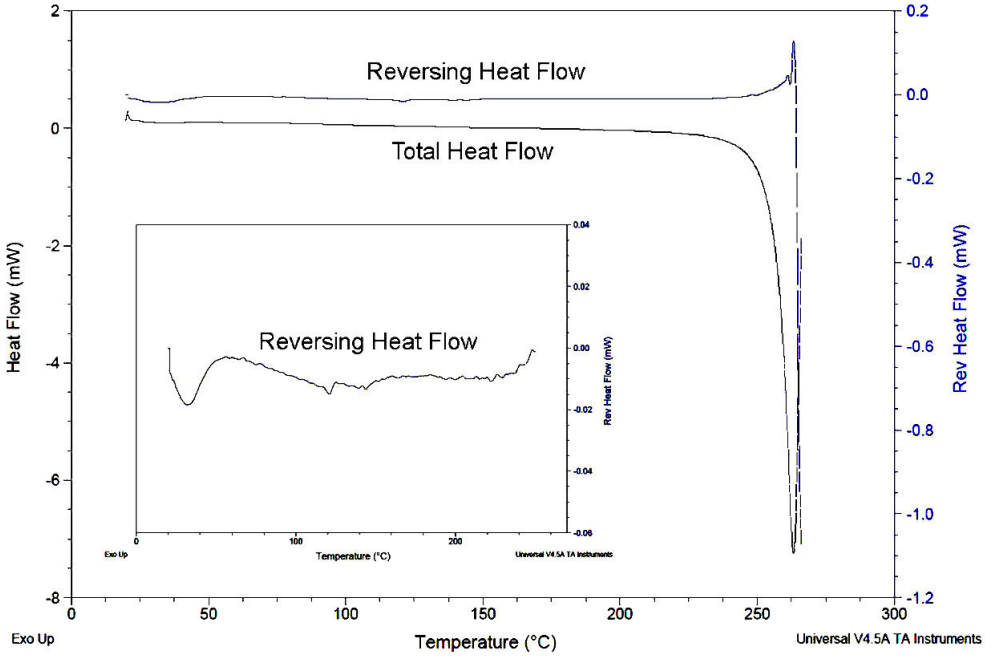

Figure 31 - mDSC result for D-methionine

Figure 32 shows the results from mDSC on two different batches of spray dried trehalose/D-methionine. The first test only showed one reversing endothermic change at around 119°C which corresponds to glass transition of amorphous trehalose content in the particles. The non-reversing endothermic change at 50°C is due to the evaporation of the water content, and the second non-reversing endothermic change indicates an enthalpic relaxation.

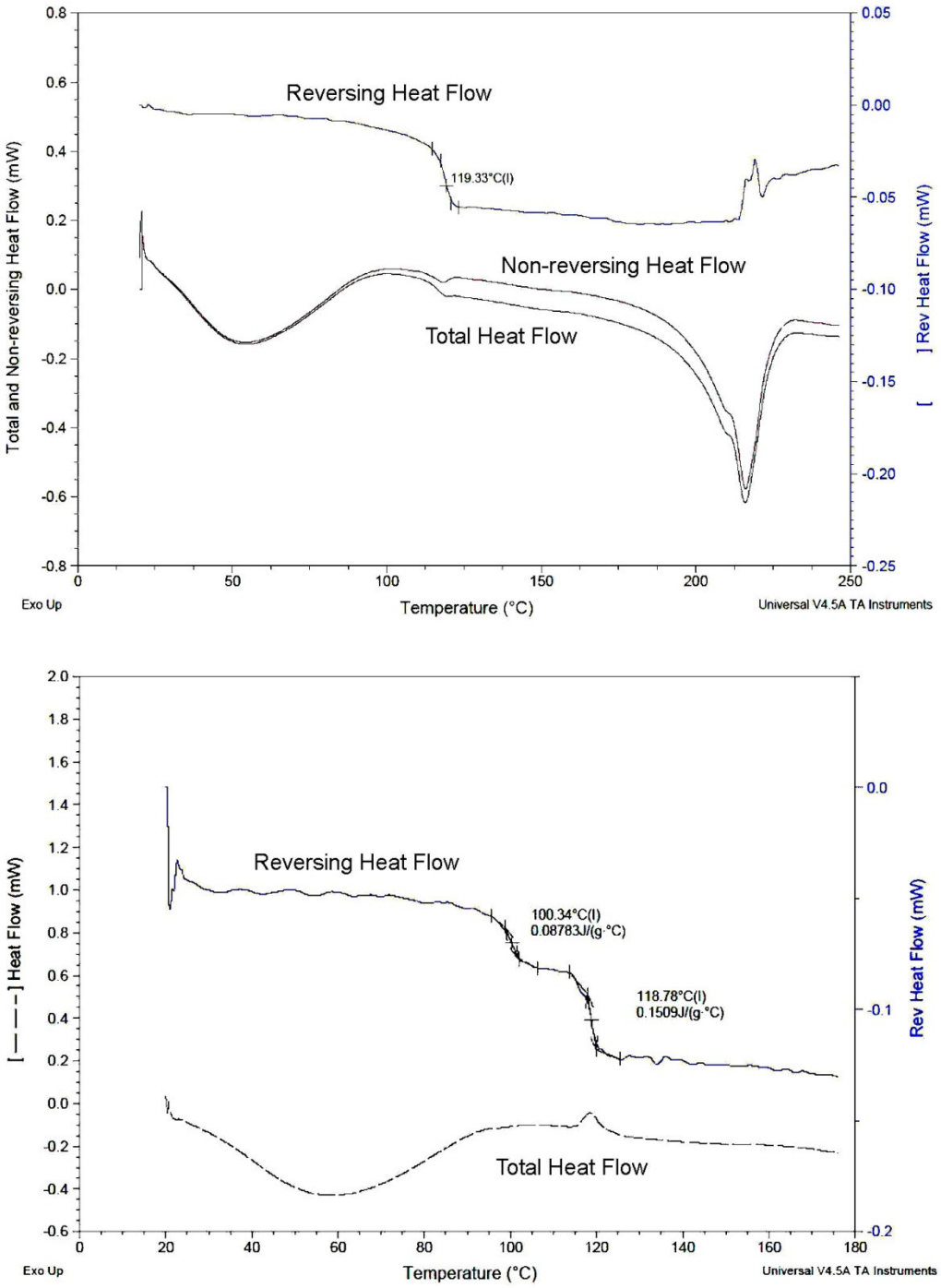

Figure 32 - mDSC results for trehalose/D-methionine

The second batch, however, had two distinctive glass transition temperatures: ~100 and ~119˚C attributing to D-methionine and trehalose respectively. The mass fractions of D-methionine and trehalose used in the two formulations were similar but they were spray dried using different spray driers: the first batch was spray dried on Büchi B-90 and the second batch on Büchi 191. This might be the reason of the different states of D-methionine. Nevertheless, it does not affect the morphology or aerosol performance of the target particle consisting of all four D-amino acids since it is going to be used only in very small mass fractions, and D-leucine is the main component contributing to the aerosol performance of the particles.

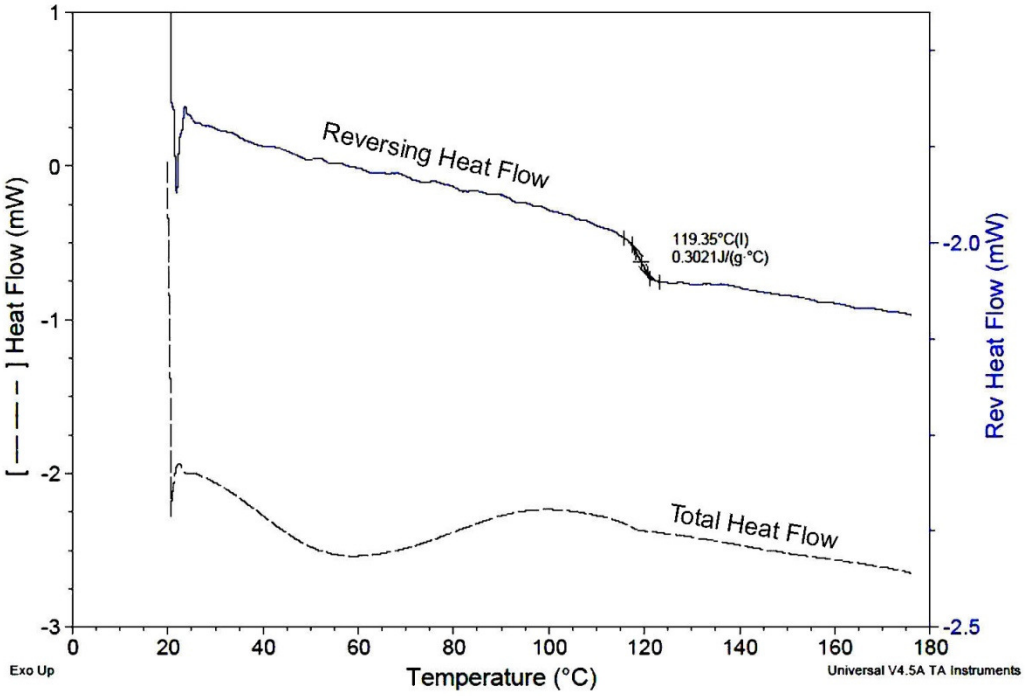

Figure 33 - mDSC result for Trehalose/D-leucine/D-methionine

The last sample consisted of trehalose, D-leucine, and D-methionine. Figure 33 shows the mDSC result for this sample. Only one glass transition temperature, i.e., that of trehalose was observed at ~119 ˚C meaning that the

D-leucine content of the particles existed in the amorphous state. The non-reversing endothermic change attributing to water content evaporation can also be seen in the mDSC curve.

Table 7 shows the summarized results of the aerodynamic diameter measurements using the APS and the aerosol performance tests. The particle size for the two formulations containing L- or D-leucine was in the desirable size range for pulmonary delivery.

Table 7 - Summary of size measurements and aerosol performance tests

Formulation	TL	TD	TDM
Particle MMAD, µm	3.82±0.04	3.25±0.03	---
Emitted mass, % of capsule mass	75.75±8.16	72.92±22.52	79.19±16.84
Lung dose fraction, % of emitted mass	63.66±16.37	62.0±7.81	36.99±14.88

Figures 34 and 35 demonstrate a representative size distribution for two powder samples: one consisting of trehalose/L-leucine and one consisting of trehalose/D-leucine. The expanded data on all the size measurements done on all of the powder samples can be found in table 8 of the appendix.

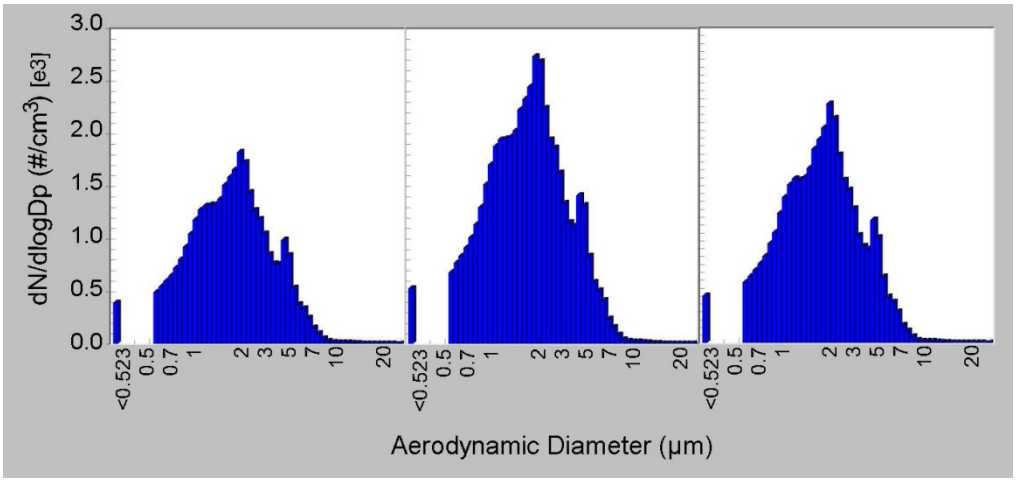

Figure 34 - Size distribution for TL

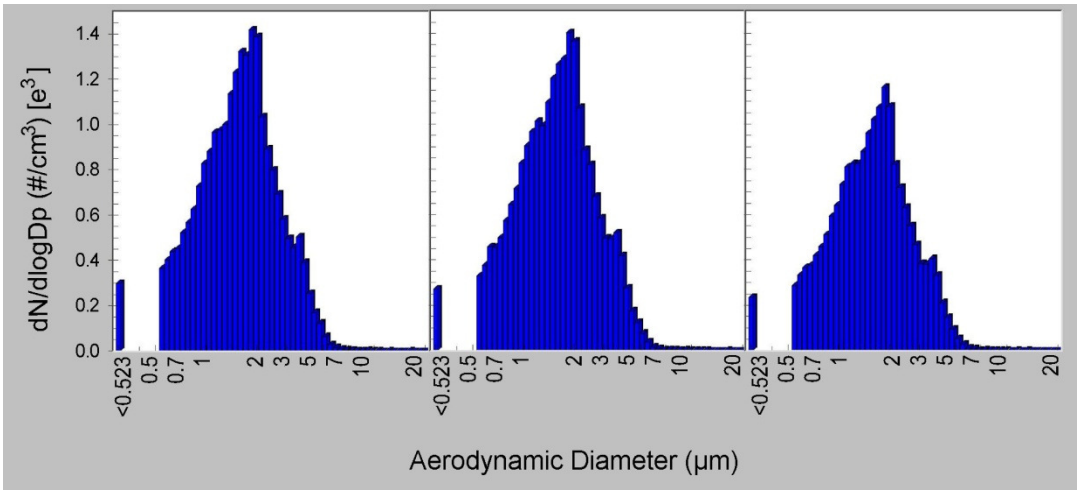

Figure 35 - Size distribution for TD

Tables 8, 9, 10, and 11 in the appendix contain all the data found in the aerosol performance tests on three formulations: L-leucine/trehalose, D-leucine/D-methionine/trehalose, and D-leucine/trehalose. More tests need to be done on the formulations with the two D-amino acids.

3.4. Conclusions

D-leucine is a suitable substitute for L-leucine in aqueous solutions for low-temperature spray drying. Aqueous solutions containing one of L- or D-leucine, trehalose, and in one case D-methionine were spray dried in order to develop respirable pharmaceutical dry powder. SEM images showed hollow and wrinkled particles for all three formulations, which is desirable for good aerosol performance of the final powder. Density measurements were done on trehalose/L and D-leucine powders, and the results were similar.

Modulated DSC and Raman spectroscopy results showed crystalline amino acids and amorphous trehalose. Both L- and D-leucine formulations had similar MMAD suitable for respiratory delivery (3.82±0.04 and 3.25±0.03 μm respectively). All lung dose fractions measured as percent of mass emitted from the capsule were acceptable (63.66±16.32%, 62.00±7.81%, and 36.99±14.86% for trehalose/L-leucine, trehalose/D-leucine, and trehalose/D-leucine/D-methionine respectively). Overall, D-leucine containing particles had very similar morphology, structure, size, density, and aerosol performance to particles containing L-leucine, which makes it a proper substitute for L-leucine in aqueous solutions for spray drying.

4. General Conclusions

This study was motivated by the growing need for effective substitutes for antibiotics considering that more and more bacteria are developing resistance to most antibiotics due to genetic mutation. Bacteriophages, as live agents each of which are active against a specific type of bacteria and can also mutate as the bacteria do, have long been considered an alternative treatment for bacterial infections.

The first part of the study investigated the feasibility of encapsulating specific bacteriophages i.e. KS4-M and KS-14 (active against *Burkholderia cepacia* complex) and a cocktail of ΦKZ/D3 (active against *P. aeruginosa*) into microparticles for respiratory delivery to treat cystic fibrosis patients. Low-temperature spray drying was done on a Büchi B-90 spray dryer with carefully determined process parameters to avoid chemical degradation of the bacteriophages. All bacteriophages were dissolved in aqueous solutions of different excipients: trehalose as a bulking agent which protects phages against thermal stress, L-leucine as dispersibility enhancer, and optionally a third excipient. Acceptable process loss (less than 1 log pfu) was achieved in all formulations. SEM images from all the resulting powders showed hollow and wrinkled particles, which is the suitable morphology for high dispersibility. The powers were also tested for aerosol performance and size distribution using an Aerolizer® inhaler and Alberta Idealized Throat or an Anderson cascade impactor. Total lung mass of 69.7% of capsule mass and MMAD of 2.5-2.8 μm was achieved for the lead formulation i.e. trehalose/L-leucine/Casein sodium. Data proved the feasibility of spray drying bacteriophages for respiratory delivery.

Since L-leucine is a nutritional source for *P. aeruginosa* biofilms in cystic fibrosis patients while D-leucine deteriorates the biofilms, the second part of the study looked into the possibility of substituting L-leucine with D-leucine in an aqueous solution of trehalose for spray drying while maintaining good aerosol performance. Considering similar physical properties of the two isomers of leucine, similar results for trehalose/L- and D-leucine particles were expected. Mass fractions used in this part of the study were the same as trehalose/L-leucine formulation in the first part i.e. 80:20% w/w, and the same process parameters were used for low-temperature spray drying. SEM images showed similar morphology for particles from the two formulations as mDSC and Raman spectroscopy results revealed similar structure: crystalline L- and D-leucine and amorphous trehalose. They also had similar MMAD (3.82±0.04 and 3.25±0.03 μm respectively) and compressed bulk density (704.8 and 725.6 kg/m^3 at 35kPa pressure respectively). The aerosol performances of both powders were similar and acceptable: 63.66±16.32 and 62.00±7.81% of capsule mass for trehalose/L- and D-leucine. The feasibility of substituting L-leucine with D-leucine was proven.

In the next step, D-methionine was added to the trehalose/D-leucine formulation in 80:10:10% w/w in an attempt to achieve a formulation containing four D-amino acids proved to be effective against *P. aeruginosa* biofilms in low concentrations. SEM images showed similar particle morphology to trehalose/D-leucine particles, mDSC and Raman spectroscopy proved the existence of crystalline D-methionine, and aerosol performance test resulted in acceptable (36.99% of capsule mass) total lung delivery.

References

[1] R. Vehring, "Pharmaceutical Particle Engineering via Spray Drying," *Pharmaceutical Research*, vol. 25, no. 5, pp. 999–1022, May 2008.

[2] J. K. Mills and D. Needham, "Targeted drug delivery," *Expert Opinion on Therapeutic Patents*, vol. 9, no. 11, pp. 1499–1513, Nov. 1999.

[3] T. Sou, E. N. Meeusen, M. de Veer, D. A. V. Morton, L. M. Kaminskas, and M. P. McIntosh, "New developments in dry powder pulmonary vaccine delivery," *Trends in Biotechnology*, vol. 29, no. 4, pp. 191–198, Apr. 2011.

[4] J. L. Rau, "The inhalation of drugs: Advantages and problems," *Respiratory Care*, vol. 50, no. 3, pp. 367–382, 2005.

[5] J. S. Patton and P. R. Byron, "Inhaling medicines: Delivering drugs to the body through the lungs," *Nature Reviews Drug Discovery*, vol. 6, no. 1, pp. 67–74, 2007.

[6] M. M. Bailey and C. J. Berkland, "Nanoparticle formulations in pulmonary drug delivery," *Medicinal Research Reviews*, vol. 29, no. 1, pp. 196–212, 2009.

[7] W. H. Finlay, *The Mechanics of Inhaled Pharmaceutical Aerosols: An Introduction*. San Diego, Academic Press, 2001.

[8] K. Masters, *Spray drying handbook*. 4th ed. New York, J. Wiley, 1985.

[9] W. R. Marshall, *Atomization and spray drying*. New York, American Institute of Chemical Engineers, 1954.

[10] "Rotary atomizers from GEA Niro." [Online]. Available: http://www.niro.com/niro/cmsdoc.nsf/webdoc/webb7ezgp8. [Accessed: 07-Mar-2013].

[11] "Atomization by GEA Niro." [Online]. Available: http://www.geaprocess.co.uk/gpuk/cmsdoc.nsf/WebDoc/webb8uje54. [Accessed: 07-Mar-2013].

[12] "Two fluid nozzle | Nozzle atomization spare parts | GEA Niro." [Online]. Available: http://www.niro.com/NIRO/cmsdoc.nsf/webdoc/webb8fvctx. [Accessed: 07-Mar-2013].

[13] "Basics of spray drying." [Online]. Available: http://www.niroinc.com/technologies/basics_of_spray_drying.asp. [Accessed: 07-Mar-2013].

[14] J. Broadhead, S. K. Edmond Rouan, and C. T. Rhodes, "The spray drying of pharmaceuticals," *Drug Development and Industrial Pharmacy*, vol. 18, no. 11–12, pp. 1169–1206, Jan. 1992.

[15] W. C. Hinds, *Aerosol technology: properties, behavior, and measurement of airborne particles*, 2nd ed. New York: Wiley, 1999.

[16] M. J. M. J. Rhodes, *Introduction to particle technology*, 2nd ed. Chichester, England; Hoboken, NJ: Wiley, 2008.

[17] P. F. DeCarlo, J. G. Slowik, D. R. Worsnop, P. Davidovits, and J. L. Jimenez, "Particle morphology and density characterization by combined

mobility and aerodynamic diameter measurements. Part 1: Theory," *Aerosol Science and Technology*, vol. 38, no. 12, pp. 1185–1205, 2004.
[18] N. A. Fuks, *Evaporation and droplet growth in gaseous media*. New York: Pergamon Press, 1959.
[19] K. . Leong, "Morphological control of particles generated from the evaporation of solution droplets: Theoretical considerations," *Journal of Aerosol Science*, vol. 18, no. 5, pp. 511–524, Oct. 1987.
[20] W. Brostow, R. Chiu, I. M. Kalogeras, and A. Vassilikou-Dova, "Prediction of glass transition temperatures: Binary blends and copolymers," *Materials Letters*, vol. 62, no. 17–18, pp. 3152–3155, Jun. 2008.
[21] Y. H. Roos, "Glass Transition Temperature and Its Relevance in Food Processing," *Annual Review of Food Science and Technology*, vol. 1, no. 1, pp. 469–496, 2010.
[22] M. G. Abiad, M. T. Carvajal, and O. H. Campanella, "A Review on Methods and Theories to Describe the Glass Transition Phenomenon: Applications in Food and Pharmaceutical Products," *Food Engineering Reviews*, vol. 1, no. 2, pp. 105–132, Aug. 2009.
[23] D. E. Dobry, D. M. Settell, J. M. Baumann, R. J. Ray, L. J. Graham, and R. A. Beyerinck, "A Model-Based Methodology for Spray-Drying Process Development," *Journal of Pharmaceutical Innovation*, vol. 4, no. 3, pp. 133–142, Sep. 2009.
[24] J. W. Ivey and R. Vehring, "The use of modeling in spray drying of emulsions and suspensions accelerates formulation and process development," *Computers & Chemical Engineering*, vol. 34, no. 7, pp. 1036–1040, Jul. 2010.
[25] D. I. Andersson and B. R. Levin, "The biological cost of antibiotic resistance," *Current Opinion in Microbiology*, vol. 2, no. 5, pp. 489–493, Oct. 1999.
[26] L. F. Mandsberg, O. Ciofu, N. Kirkby, L. E. Christiansen, H. E. Poulsen, and N. Høiby, "Antibiotic Resistance in Pseudomonas aeruginosa Strains with Increased Mutation Frequency Due to Inactivation of the DNA Oxidative Repair System," *Antimicrob. Agents Chemother.*, vol. 53, no. 6, pp. 2483–2491, Jun. 2009.
[27] K. D. Seed and J. J. Dennis, "Isolation and characterization of bacteriophages of the Burkholderia cepacia complex," *FEMS Microbiology Letters*, vol. 251, no. 2, pp. 273–280, 2005.
[28] R. R. Reinert, "The antimicrobial resistance profile of Streptococcus pneumoniae," *Clinical Microbiology and Infection*, vol. 15, pp. 7–11, 2009.
[29] S. T. Abedon and C. Thomas-Abedon, "Phage therapy pharmacology," *Current Pharmaceutical Biotechnology*, vol. 11, no. 1, pp. 28–47, Jan. 2010.
[30] L. Broxmeyer, "Bacteriophages: Antibacterials with a future?," *Medical Hypotheses*, vol. 62, no. 6, pp. 889–893, 2004.
[31] M. Kutateladze and R. Adamia, "Bacteriophages as potential new therapeutics to replace or supplement antibiotics," *Trends in Biotechnology*, vol. 28, no. 12, pp. 591–595, Dec. 2010.

[32] A. b. Monk, C. d. Rees, P. Barrow, S. Hagens, and D. r. Harper, "Bacteriophage applications: where are we now?," *Letters in Applied Microbiology*, vol. 51, no. 4, pp. 363–369, 2010.
[33] T. Häusler, "Antibacterial Phage Therapy - The Naked Scientists 2007.05.21," *The Naked Scientists: Science Radio & Science Podcasts*. [Online]. Available: http://www.thenakedscientists.com/HTML/articles/article/virusesvssuperbugs/. [Accessed: 20-Nov-2012].
[34] S. Hoe, D. D. Selmer, A. D. Goudie, K. H. Lynch, S. Matinkhoo, W. H. Finlay, J. J. Dennis, and R. Vehring, "Respirable bacteriophages for the treatment of lung infections," *Journal of Aerosol Medicine and Pulmonary Drug Delivery*, Manuscript submitted for publication.
[35] "Information about Bacteriophages." [Online]. Available: http://www.phages.org/PhageInfo.html. [Accessed: 05-Apr-2013].
[36] L. Golshahi, K. D. Seed, J. J. Dennis, and W. H. Finlay, "Toward modern inhalational bacteriophage therapy: nebulization of bacteriophages of Burkholderia cepacia complex," *Journal of Aerosol Medicine and Pulmonary Drug Delivery*, vol. 21, no. 4, pp. 351–360, Dec. 2008.
[37] M. Müller-Merbach, T. Rauscher, and J. Hinrichs, "Inactivation of bacteriophages by thermal and high-pressure treatment," *International Dairy Journal*, vol. 15, no. 6–9, pp. 777–784, Jun. 2005.
[38] M. C. Chopin, "Resistance of 17 mesophilic lactic Streptococcus bacteriophages to pasteurization and spray-drying," *Journal of Dairy Research*, vol. 47, no. 1, pp. 131–139, Feb. 1980.
[39] S. Matinkhoo, K. H. Lynch, J. J. Dennis, W. H. Finlay, and R. Vehring, "Spray-dried respirable powders containing bacteriophages for the treatment of pulmonary infections," *Journal of Pharmaceutical Sciences*, vol. 100, no. 12, pp. 5197–5205, 2011.
[40] L. Golshahi, K. h. Lynch, J. j. Dennis, and W. h. Finlay, "In vitro lung delivery of bacteriophages KS4-M and ΦKZ using dry powder inhalers for treatment of Burkholderia cepacia complex and Pseudomonas aeruginosa infections in cystic fibrosis," *Journal of Applied Microbiology*, vol. 110, no. 1, pp. 106–117, 2011.
[41] G. M. Sastry and N. Agmon, "Trehalose prevents myoglobin collapse and preserves its internal mobility," *Biochemistry*, vol. 36, no. 23, pp. 7097–7108, Jun. 1997.
[42] M. Ameri and Y.-F. Maa, "Spray Drying of Biopharmaceuticals: Stability and Process Considerations," *Drying Technology*, vol. 24, no. 6, pp. 763–768, 2006.
[43] T. Tarara, C. Stevenson, S. Thompson, R. Vehring, and N. Sadrzadeh, "Methionine-Containing Protein or Peptide Compositions and Methods of Making and Using," U.S. Patent WO/2007/09528824-Aug-2007.
[44] L. M. Crowe, D. S. Reid, and J. H. Crowe, "Is trehalose special for preserving dry biomaterials?," *Biophysics Journal*, vol. 71, no. 4, pp. 2087–2093, Oct. 1996.

[45] J. Raula, F. Thielmann, M. Naderi, V.-P. Lehto, and E. I. Kauppinen, "Investigations on particle surface characteristics vs. dispersion behaviour of L-leucine coated carrier-free inhalable powders," *International Journal of Pharmaceutics*, vol. 385, no. 1–2, pp. 79–85, Jan. 2010.
[46] T. P. Learoyd, J. L. Burrows, E. French, and P. C. Seville, "Sustained delivery by leucine-modified chitosan spray-dried respirable powders," *International Journal of Pharmaceutics*, vol. 372, no. 1–2, pp. 97–104, May 2009.
[47] M. Müller-Merbach, H. Neve, and J. Hinrichs, "Kinetics of the thermal inactivation of the Lactococcus lactis bacteriophage P008," *Journal of Dairy Research*, vol. 72, no. 3, pp. 281–286, Aug. 2005.
[48] A. L. Feng, M. A. Boraey, M. A. Gwin, P. R. Finlay, P. J. Kuehl, and R. Vehring, "Mechanistic models facilitate efficient development of leucine containing microparticles for pulmonary drug delivery," *International Journal of Pharmaceutics*, vol. 409, no. 1–2, pp. 156–163, May 2011.
[49] B. M. Ibrahim, S. W. Jun, M. Y. Lee, S. H. Kang, and Y. Yeo, "Development of inhalable dry powder formulation of basic fibroblast growth factor," *International Journal of Pharmaceutics*, vol. 385, no. 1–2, pp. 66–72, Jan. 2010.
[50] J. Raula, J. A. Kurkela, D. P. Brown, and E. I. Kauppinen, "Study of the dispersion behaviour of l-leucine containing microparticles synthesized with an aerosol flow reactor method," *Powder Technology*, vol. 177, no. 3, pp. 125–132, 2007.
[51] S. H. Lee, D. Heng, W. K. Ng, H.-K. Chan, and R. B. H. Tan, "Nano spray drying: A novel method for preparing protein nanoparticles for protein therapy," *International Journal of Pharmaceutics*, vol. 403, no. 1–2, pp. 192–200, Jan. 2011.
[52] C. Arpagaus, "A Novel Laboratory-Scale Spray Dryer to Produce Nanoparticles," *Drying Technology*, vol. 30, no. 10, pp. 1113–1121, 2012.
[53] S. P. NEWMAN and W. W. BUSSE, "Evolution of dry powder inhaler design, formulation, and performance," *Respiratory Medicine*, vol. 96, no. 5, pp. 293–304, May 2002.
[54] E. A. Bronsky, J. Grossman, M. J. Henis, P. P. Gallo, U. Yegen, G. Della Cioppa, J. Kottakis, and S. Mehra, "Inspiratory flow rates and volumes with the Aerolizer dry powder inhaler in asthmatic children and adults," *Current Medical Research Opinion*, vol. 20, no. 2, pp. 131–137, 2004.
[55] E. Morello, E. Saussereau, D. Maura, M. Huerre, L. Touqui, and L. Debarbieux, "Pulmonary bacteriophage therapy on Pseudomonas aeruginosa cystic fibrosis strains: first steps towards treatment and prevention," *PLoS ONE*, vol. 6, no. 2, p. e16963, 2011.
[56] A. Wright, C. H. Hawkins, E. E. Anggård, and D. R. Harper, "A controlled clinical trial of a therapeutic bacteriophage preparation in chronic otitis due to antibiotic-resistant Pseudomonas aeruginosa; a preliminary report of efficacy," *Clinical Otolaryngology*, vol. 34, no. 4, pp. 349–357, Aug. 2009.

[57] I. Kolodkin-Gal, D. Romero, S. Cao, J. Clardy, R. Kolter, and R. Losick, "D-amino acids trigger biofilm disassembly," *Science*, vol. 328, no. 5978, pp. 627–629, Apr. 2010.
[58] D. Lopez, H. Vlamakis, and R. Kolter, "Generation of multiple cell types in Bacillus subtilis," *FEMS Microbiology Reviews*, vol. 33, no. 1, pp. 152–163, Jan. 2009.
[59] E. Karatan and P. Watnick, "Signals, regulatory networks, and materials that build and break bacterial biofilms," *Microbiology and Molecular Biology Reviews*, vol. 73, no. 2, pp. 310–347, Jun. 2009.
[60] M. E. Olson, H. Ceri, D. W. Morck, A. G. Buret, and R. R. Read, "Biofilm bacteria: formation and comparative susceptibility to antibiotics," *Canadian Journal of Veterinary Research*, vol. 66, no. 2, pp. 86–92, Apr. 2002.
[61] K. Lewis, "Persister cells, dormancy and infectious disease," *Nature Reviews Microbiology*, vol. 5, no. 1, pp. 48–56, Jan. 2007.
[62] K. Lewis, "Persister cells," *Annual Review of Microbiology*, vol. 64. pp. 357-372, 2010.
[63] D. López, H. Vlamakis, and R. Kolter, "Biofilms," *Cold Spring Harbor Perspectives in Biology*, vol. 2, no. 7, Jul. 2010.
[64] C. A. Gordon, N. A. Hodges, and C. Marriott, "Antibiotic interaction and diffusion through alginate and exopolysaccharide of cystic fibrosis-derived Pseudomonas aeruginosa," *Journal of Antimicrobial Chemotherapy*, vol. 22, no. 5, pp. 667–674, Nov. 1988.
[65] N. A. Hodges and C. A. Gordon, "Protection of Pseudomonas aeruginosa against ciprofloxacin and beta-lactams by homologous alginate.," *Antimicrobial Agents and Chemotherapy*, vol. 35, no. 11, pp. 2450–2452, Nov. 1991.
[66] D. G. Allison and M. J. Matthews, "Effect of polysaccharide interactions on antibiotic susceptibility of Pseudomonas aeruginosa," *Journal of Applied Bacteriology*, vol. 73, no. 6, pp. 484–488, Dec. 1992.
[67] N. Bolister, M. Basker, N. A. Hodges, and C. Marriott, "The diffusion of β-lactam antibiotics through mixed gels of cystic fibrosis-derived mucin and Pseudomonas aeruginosa alginate," *Journal of Antimicrobial Chemotherapy*, vol. 27, no. 3, pp. 285–293, Mar. 1991.
[68] N. Bagge, M. Schuster, M. Hentzer, O. Ciofu, M. Givskov, E. P. Greenberg, and N. Høiby, "Pseudomonas aeruginosa Biofilms Exposed to Imipenem Exhibit Changes in Global Gene Expression and β-Lactamase and Alginate Production," *Antimicrobial Agents and Chemotherapy*, vol. 48, no. 4, pp. 1175–1187, Apr. 2004.
[69] N. Høiby, "New antimicrobials in the management of cystic fibrosis," *Journal of Antimicrobial Chemotherapy*, vol. 49, no. 2, pp. 235–238, Feb. 2002.
[70] G. Doring, S. P. Conway, H. G. Heijerman, M. E. Hodson, N. Hoiby, A. Smyth, and D. J. Touw, "Antibiotic therapy against Pseudomonas aeruginosa in cystic fibrosis: a European consensus," *European Respiratory Journal*, vol. 16, no. 4, pp. 749–767, Oct. 2000.

[71] N. Høiby, H. K. Johansen, C. Moser, O. Ciofu, P. Ø. Jensen, M. Kolpen, L. Mandsberg, M. Givskov, S. Molin, and T. Bjarnsholt, "Pseudomonas aeruginosa Biofilms in the Lungs of Cystic Fibrosis Patients," in *Biofilm infections*, New York: Springer, 2011.
[72] T. Bjarnsholt, P. Ø. Jensen, M. J. Fiandaca, J. Pedersen, C. R. Hansen, C. B. Andersen, T. Pressler, M. Givskov, and N. Høiby, "Pseudomonas aeruginosa biofilms in the respiratory tract of cystic fibrosis patients," *Pediatric Pulmonology*, vol. 44, no. 6, pp. 547–558, 2009.
[73] J. B. Lyczak, C. L. Cannon, and G. B. Pier, "Lung Infections Associated with Cystic Fibrosis," *Clinical Microbiology Reviews*, vol. 15, no. 2, pp. 194–222, Apr. 2002.
[74] K. L. Palmer, L. M. Aye, and M. Whiteley, "Nutritional Cues Control Pseudomonas aeruginosa Multicellular Behavior in Cystic Fibrosis Sputum," *Journal of Bacteriology*, vol. 189, no. 22, pp. 8079–8087, Nov. 2007.
[75] K. L. Palmer, L. M. Mashburn, P. K. Singh, and M. Whiteley, "Cystic Fibrosis Sputum Supports Growth and Cues Key Aspects of Pseudomonas aeruginosa Physiology," *Journal of Bacteriology*, vol. 187, no. 15, pp. 5267–5277, Aug. 2005.
[76] A. L. Jenkins, R. A. Larsen, and T. B. Williams, "Characterization of amino acids using Raman spectroscopy," *Spectrochimica Acta Part A: Molecular and Biomolecular Spectroscopy*, vol. 61, no. 7, pp. 1585–1594, May 2005.
[77] F. Cava, H. Lam, M. A. de Pedro, and M. K. Waldor, "Emerging knowledge of regulatory roles of D-amino acids in bacteria," *Cellular and Molecular Life Sciences*, vol. 68, no. 5, pp. 817–831, Mar. 2011.
[78] "an introduction to amino acids." [Online]. Available: http://www.chemguide.co.uk/organicprops/aminoacids/background.html. [Accessed: 12-Feb-2013].
[79] S. P. Bernier, D.-G. Ha, W. Khan, J. H. Merritt, and G. A. O'Toole, "Modulation of Pseudomonas aeruginosa surface-associated group behaviors by individual amino acids through c-di-GMP signaling," *Research in Microbiology*, vol. 162, no. 7, pp. 680–688, Sep. 2011.
[80] M. Friedman, "Origin, microbiology, nutrition, and pharmacology of D-amino acids," *Chemistry & Biodiversity*, vol. 7, no. 6, pp. 1491–1530, Jun. 2010.
[81] H. Lam, D.-C. Oh, F. Cava, C. N. Takacs, J. Clardy, M. A. de Pedro, and M. K. Waldor, "D-Amino Acids Govern Stationary Phase Cell Wall Remodeling in Bacteria," *Science*, vol. 325, no. 5947, pp. 1552–1555, Sep. 2009.
[82] Y. L. Huijuan Xu, "d-Amino acid mitigated membrane biofouling and promoted biofilm detachment," *Journal of Membrane Science*, vol. 376, pp. 266–274.
[83] "WO2011085326A1 D- AMINO ACIDS FOR USE IN TREATING BIOFILMS," *wPATtc*. [Online]. Available: http://w.pat.tc/WO2011085326A1. [Accessed: 20-Dec-2012].
[84] *CRC Handbook of Chemistry and Physics, 94th Edition - CRC Press Book*. .

[85] A. Shamsaddini-Shahrbabak and R. Vehring, "The Compression Behavior of Respirable Powders at Different Relative Humidity Measured by a Compressed Bulk Density Tester for Small Sample Masses," *Respiratory Drug Delivery*, Arizona, 2012 [Online]. Available: http://www.rddonline.com/publications/articles/article.php?ArticleID=1782. [Accessed: 13-Mar-2013].

[86] R. Vehring, "Red-excitation dispersive Raman spectroscopy is a suitable technique for solid-state analysis of respirable pharmaceutical powders," *Applied Spectroscopy*, vol. 59, no. 3, pp. 286–292, Mar. 2005.

[87] F. Sussich, R. Urbani, F. Princivalle, and A. Cesàro, "Polymorphic Amorphous and Crystalline Forms of Trehalose," *Journal of American Chemical Society*, vol. 120, no. 31, pp. 7893–7899, Aug. 1998.

[88] F. Sussich, C. Skopec, J. Brady, and A. Cesàro, "Reversible dehydration of trehalose and anhydrobiosis: from solution state to an exotic crystal?," *Carbohydrate Research*, vol. 334, no. 3, pp. 165–176, Aug. 2001.

[89] R. Surana, A. Pyne, M. Rani, and R. Suryanarayanan, "Measurement of enthalpic relaxation by differential scanning calorimetry—effect of experimental conditions," *Thermochimica Acta*, vol. 433, no. 1–2, pp. 173–182, Aug. 2005.

Appendix

Table 8 - Details of size measurement data

	Count Distribution			Average	St Deviation	Mass Distribution			Average	St Deviation
Trehalose										
Median (µm)	1.9	1.9	---	1.9	0.00	4.14	4.27	---	4.205	0.09
Mean (µm)	2.16	2.17	---	2.165	0.00	4.62	5.16	---	4.89	0.38
Geometric mean (µm)	1.85	1.86	---	1.855	0.00	4.1	4.42	---	4.26	0.22
Geometric St Deviation	1.76	1.75	---	1.755	0.00	1.61	1.72	---	1.665	0.07
Trehalose/D-Leucine										
Median (µm)	1.58	1.59	1.57	1.58	0.01	3.23	3.29	3.24	3.25	0.03
Mean (µm)	1.75	1.77	1.75	1.76	0.01	3.37	3.44	3.31	3.37	0.07
Geometric mean (µm)	1.54	1.55	1.54	1.54	0.01	3.05	3.11	3.03	3.06	0.04
Geometric St Deviation	1.66	1.66	1.66	1.66	0.00	1.56	1.56	1.53	1.55	0.02
Trehalose/L-Leucine										
Median (µm)	1.64	1.67	1.66	1.66	0.02	3.81	3.86	3.78	3.82	0.04
Mean (µm)	1.9	1.93	1.9	1.91	0.02	4.23	4.31	4.15	4.23	0.08
Geometric mean (µm)	1.63	1.65	1.63	1.64	0.01	3.75	3.81	3.69	3.75	0.06
Geometric St Deviation	1.74	1.74	1.73	1.74	0.01	1.63	1.64	1.62	1.63	0.01

Table 9 - Details of aerosol performance, LT formulations

	Loaded dose (mg)	Leu throat mass (mg)	Leu filter mass (mg)	Emitted mass (% of capsule load)	Lung dose (% of emitted mass)	Lung dose (% of capsule load)
Trehalose/ L-Leu	20.2	1.54	1.15	66.58	42.75	28.47
	20.3	1.6	1.22	69.46	43.26	30.05
	20.6	1.77	1.29	74.27	42.16	31.31
	22.29	0.44	2.53	66.62	85.19	56.75
	19.29	0.85	2.27	80.87	72.76	58.84
	20.02	0.62	2.36	74.43	79.19	58.94
	21.54	0.68	2.89	82.87	80.95	67.08
	22.52	1.43	2.77	93.25	65.95	61.50
	19.26	1.09	1.83	75.80	62.67	47.51
	19.96	1.12	1.81	73.40	61.77	45.34
Average	20.60	1.11	2.01	75.75	63.66	48.57
St Deviation	1.15	0.46	0.64	8.16	16.37	14.32

Table 10 - Details of aerosol performance, DMT formulations

	Loaded dose (mg)	Leu throat mass (mg)	Leu filter mass (mg)	Emitted mass (% of capsule load)	Lung dose (% of emitted mass)	Lung dose (% of capsule load)
Trehalose/ D-Leu/D-Met	19.58	1.77	1.3	86.56	42.34	33.19
	19.54	1.45	1.62	53.99	52.76	41.45
	21.94	3.14	0.66	91.61	17.36	15.04
	19.7	1.6	0.88	72.58	35.48	22.33
Average	20.19	1.99	1.11	76.19	36.99	28.00
St Deviation	1.168	0.77	0.42	16.84	14.88	11.66

Table 11 - Details of Aerosol performance, DT formulations

	Loaded dose (mg)	Leu throat mass (mg)	Leu filter mass (mg)	Emitted mass (% of capsule load)	Lung dose (% of emitted mass)	Lung dose (% of capsule load)
Trehalose/ D-Leu	21.20	0.92	1.42	55.19	60.68	33.49
	21.50	1.18	1.72	67.44	59.31	40.00
	21.10	1.44	1.98	81.04	57.89	46.92
	20.00	0.92	1.37	71.56	59.83	42.81
	19.80	0.94	1.46	75.76	60.83	46.09
	20.70	1.04	1.26	69.44	54.78	38.04
	20.10	1.21	1.04	55.97	46.22	25.87
	19.90	0.63	0.89	38.19	58.55	22.36
	21.20	0.28	0.66	22.17	70.21	15.57
	21.09	0.95	1.89	67.33	66.55	44.81
	20.98	1.83	2.14	94.61	53.90	51.00
	19.94	1.21	1.69	72.72	58.28	42.38
	22.10	0.81	3.43	95.93	80.90	77.60
	21.40	1.28	2.82	95.79	68.78	65.89
	20.10	1.02	1.68	67.16	62.22	41.79
	19.60	1.36	2.82	106.63	67.46	71.94
	20.63	1.37	2.87	102.76	67.69	69.56
Average	20.67	1.08	1.83	72.92	62.00	45.65
St Deviation	0.72	0.34	0.77	22.52	7.81	17.38